Conceptual models of dissolved carbon fluxes in a two-layer stratified lake: interannual typhoon responses under extreme climates

Hao-Chi Lin[1], Keisuke Nakayama[2], Jeng-Wei Tsai[3], and Chih-Yu Chiu[4]

[1] Department of Geography, National Taiwan University, Taipei City, Taiwan

[2] Graduate School of Engineering, Kobe University, Kobe City, Japan

[3] Graduate Institute of Bioresources, National Pingtung University of Science and Technology, Pingtung, Taiwan

[4] Biodiversity Research Center, Academia Sinica, Taipei City, Taiwan

* Corresponding author: Keisuke Nakayama (nakayama@phoenix.kobe-u.ac.jp)

14   **Abstract**

15   Extreme climates affect the seasonal and interannual patterns of carbon (C) distribution

16   in lentic ecosystems due to the regimes of river inflow and thermal stratification. Typhoons

17   rapidly load substantial amounts of terrestrial C into smaller subtropical lakes (i.e., Yuan-Yang

18   Lake, YYL, Taiwan), renewing and mixing the water column. We developed a conceptual

19   dissolved C model and hypothesized that allochthonous C loading and river inflow intrusion may

20   affect the dissolved inorganic C (DIC) and dissolved organic C (DOC) distributions in a small

21   subtropical lake under these extreme climates. A two-layer conceptual C model was developed to

22   explore how the DIC and DOC fluxes respond to typhoon disturbances on seasonal and

23   interannual time scales in YYL while simultaneously considering autochthonous processes such

24   as algal photosynthesis, remineralization, and vertical transformation. To compare the temporal

25   patterns of fluxes between typhoon years (2015–2016) and non-typhoon years (2017–2018),

26   monthly field samples were obtained and their DIC, DOC, and chlorophyll a concentrations

27   measured. The results demonstrated that net ecosystem production was 3.14 times higher in the

28   typhoon years than in the non-typhoon years. This results suggested that a loading of

29   allochthonous C was the most crucial driver of the temporal variation of C fluxes in the typhoon

30   years because of changes in physical and biochemical processes, such as photosynthesis,

31   mineralization, and vertical transportation. However, the lowered vertical transportation rate

32   shaped the seasonal C in the non-typhoon years due to thermal stratification within this small

33   subtropical lake.

1. Introduction

The Intergovernmental Panel for Environmental Changes Sixth Assessment Report (IPCC AR6) (2021) suggested that, by 2050, not only is air temperature going to increase by at least about 1.5°C but high-intensity storms and drought events will become more frequent as a result of global warming and climate change. In freshwater ecosystems, extreme climates may change the mixing regimes of freshwater columns (Kraemer et al., 2021; Maberly et al., 2020; Woolway et al., 2020), heat wave events (Woolway et al., 2021a; Woolway et al., 2021b), droughts (Marcé et al., 2019), and floods (Woolway et al., 2018). Freshwater ecosystems store around 0.32 to 1.8 Pg C yr^{-1}, which is approximately equivalent to shallow coastal areas. Freshwater ecosystems provide important services for human sustainability, such as acting as processing hotspots in regional carbon (C) cycling (Aufdenkampe et al., 2011; Cole et al., 2007; Engel et al., 2018; Lauerwald et al., 2015; Raymond et al., 2013). Extreme weather events might induce stronger seasonal thermal stratification from spring to summer and longer overturns from autumn to winter, thereby changing C distribution and transportation within water bodies (Kraemer et al., 2021; Olsson et al., 2022a; Woolway et al., 2020). The responses of C fluxes in small lakes (lake area < 1 km^2) are sensitive to climate change due to the ease with which C mixes within water columns (Doubek et al., 2021; MacIntyre et al., 2021; Winslow et al., 2015). Moreover, storms induce dramatic changes in thermal stratification and water inflows (Lin et al., 2022; Olsson et al., 2022b; Vachon and Del Giorgio, 2014; Woolway et al., 2018). River inflows and wind turbulence released allochthonous C from sediments into the water column after storm events in small stratified lakes (Bartosiewicz et al., 2015; Czikowsky et al., 2018; Vachon and Del Giorgio, 2014). However, small lakes account for 25% to 35% of the total area of the earth's surface lakes (Cole et al., 2007; Downing et al., 2006; Raymond et al., 2013). Compared to the case in larger lakes, our understanding of C fluxes in small lakes remain uncertain because small lakes have usually been ignored in calculations of C fluxes on a global scale (Cole et al., 2007; Raymond et al., 2013). Thus, elucidation of the C fluxes in small lakes in extreme weathers conditions is key to optimizing estimations of global C fluxes in extreme climates.

Understanding the influences of physical, hydrological, and biogeochemical processes on the fate of C fluxes in smaller lake ecosystems is challenging work (Aufdenkampe et al., 2011; Cole et al., 2007; Raymond et al., 2013; Tranvik et al., 2009; Vachon et al., 2021; Woolway et al., 2018). Not only is measurement difficult, but so in the elucidation of the dynamics and interactions between factors and processes associated with C fluxes. Dissolved inorganic carbon (DIC) concentration is an important factor in estimating CO_2 fluxes within lake ecosystems (Smith, 1985). Among C fluxes in a freshwater body, the partial pressure of CO_2 (pCO_2), defined as CO_2 emission across the air–water interface, is affected by DIC, water

71 temperature, wind speed, and pH (Jähne et al., 1987; Smith, 1985). River inflows, sediment C

72 burial, and heterotrophic respiration in the water column contribute to DIC dynamics in lakes

73 (Hope et al., 2004; Vachon et al., 2021); simultaneously, autotrophic organisms, such as

74 plankton and submerged vegetation, capture DIC via photosynthesis (Amaral et al., 2022;

75 Nakayama et al., 2020; Nakayama et al., 2022). Moreover, calcification and mineralization may

76 consume dissolved oxygen within water, inducing uncertainty in pCO_2 estimation (Hanson et al.,

77 2015; Lin et al., 2022; Nakayama et al., 2022). Dissolved organic carbon (DOC) might

78 contribute to CO_2 emission from lake water to the atmosphere through mineralization and

79 remineralization within lake ecosystems (Hanson et al., 2015; Sobek et al., 2005). In subtropical

80 freshwater ecosystems, DOC concentration is a vital factor in describing variances in

81 mineralization and remineralization rates for dissolved C (Lin et al., 2022; Shih et al., 2019).

82   Typhoons might significantly impact C distributions within the water columns in

83 subtropical regions (Chiu et al., 2020; Lin et al., 2022). Kossin et al. (2013) investigated global

84 storm events with an accumulated rainfall of about 50 mm, which accounts for approximately

85 10 %–40% of precipitation in a subtropical typhoon event. Some studies found not only that

86 extreme rainstorms would impact the dissolved carbon in large lakes and catchments due to

87 weathering (Sun et al., 2021; Zhou et al., 2023) but also that typhoon disturbances quickly mix,

88 renew, or dilute the water in small subtropical lakes (Kimura et al., 2012; Kimura et al., 2017;

89 Lin et al., 2022). However, the complex interactions between biogeochemical and physical

90 regimes for autochthonous and allochthonous C introduce uncertainty in elucidating the

91 complete patterns between typhoons and dissolved C concentrations in small subtropical lakes.

92 This uncertainty hinders our understanding of the seasonal and interannual variations in DIC

93 and DOC concentrations (Lin et al., 2022). Thus, to understand the seasonal regimes and to

94 estimate C fluxes in subtropical lakes, we investigated the variations inof DIC and DOC due to

95 typhoon disturbances.

96   Typhoons' effects on C fluxes were previously studied in a small, two-layer stratified,

97 subtropical lake, Yuan–Yang Lake (YYL) in Taiwan (Chiu et al., 2020; Jones et al., 2009; Lin et

98 al., 2021; Lin et al., 2022). Jones et al. (2009) used the conceptual hydrology model and sensor

99 data to estimate CO_2 emission in YYL during typhoon disturbances that occurred in October

100 2004: 2.2 to 2.7 g C m^{-2} d^{-1} of CO_2 was released into the atmosphere. CO_2 emissions into the

101 atmosphere were recorded at around 3.0 to 3.7 g C m^{-2} d^{-1} because of substantial loads of

102 terrestrial C via river inflows after strong typhoons in YYL (Chiu et al., 2020).In particular,

103 vertical mixing, thermal stratification, and river retention regimes were found to be essential

104 physical processes in the C fluxes in YYL (Lin et al., 2021; Lin et al., 2022). The results of

105 these studies suggest that river intrusion and thermal stratification are key factors shaping the

106 seasonal and interannual patterns of C fluxes during typhoon disturbances. River intrusion

107   controls not only the C fluxes, algal biomass, and nutrient loading, but also influences the length

108   of stratification and hydraulic retention times (Lin et al., 2021; Lin et al., 2022; Maranger et al.,

109   2018; Nakayama et al., 2020; Olsson et al., 2022a; Olsson et al., 2022b; Zwart et al., 2017;

110   Vachon and Del Giorgio, 2014). Therefore, we hypothesized that allochthonous C loading and

111   river inflow intrusion might affect DIC and DOC distributions. Further, autochthonous

112   processes in small subtropical lakes, such as algal photosynthesis, remineralization, and vertical

113   transportation, must also be considered. Here, we tested our hypothesis developing two-layer

114   conceptual C models to assess C flux responses to typhoon disturbances in small subtropical

115   lakes.

116

117   2.   Materials and methods

118   *2.1*   *Study site*

119   YYL is a shallow (mean water depth: 4.3 m) and oligotrophic (total phosphorous: 10-

120   20 μg-P L^{-1}; total nitrogen: 20-60 μg-N L^{-1}) subtropical mountain lake (Chou et al., 2000; Tsai

121   et al., 2008; Wu et al., 2001) on Chi-Lan Mountain at around 1,640 asl in north-central Taiwan

122   (24.58° N, 121.40° E) (Fig. 1). Its water is brown because of its humic acid content (colored

123   dissolved organic matter: 20–50 ppb QSE; with specific ultraviolet absorbance at 254 nm

124   assessed by a portable fluorometer (model C3; Turner Designs, Sunnyvale, CA, USA); mean

125   pH: 5.4). YYL is surrounded by old-growth trees such as *Chamaecyparis formosensis*,

126   *Chamaecyparis obtusa* var. *formosana*, and *Rhododendron formosanum* Heiml (Chou et al.,

127   2000). Precipitation is over 3,000 mm yr^{-1}, and typhoon precipitation contributes up to half of

128   the total precipitation in YYL (Chang et al., 2007; Lai et al., 2006). Due to the rapid renewal of

129   the water body, the water retention time (or residence time) was around 4.4 days in typhoon

130   Megi from 27 September to 1 October 2016 (Lin et al., 2022). The water surface temperature

131   ranges from 15 to 25 °C during March to August, and the water column overturns in September

132   (Kimura et al., 2012; Kimura et al., 2017; Lin et al., 2021). The concentrations of DIC, DOC

133   (Lin et al., 2021), total nitrogen, total phosphate (Chiu et al., 2020; Tsai et al., 2008) and

134   bacteria compositions (Shade et al., 2011) increase within YYL from autumn to winter. YYL has

135   been registered as a long-term ecological study site by the Ministry of Science and Technology

136   (MOST) of Taiwan since 1992 and it became part of the Global Lake Ecological Observatory

137   Network (GLEON) in 2004.

138

139   *2.2*   *Water sampling and chemical analysis*

140   We collected water quality samples (DOC, DIC, and Chl. *a*) at water depths of 0.04,

141   0.50, 1.00, 2.00, and 3.50 m at the buoy site (Fig. 1). From January 2015 to December 2018, we

measured the water surfaces for six river inflows and one outflow each month using a horizontal van Dorn bottle (2.20 L, acrylic) (Fig. 1). These samples were collected using a portable hand pump and glass microfiber filter papers (47 mm GF/F, nominal pore size 0.70 μm; Whatman, Maidstone, Kent, UK) to obtain filtrate samples. Water samples were stored at around 4°C in a refrigerator until analysis. Samples were analyzed using an infrared gas detector to detect DIC and DOC concentrations with persulfate digestion (model 1088 Rotary TOC autosampler; OI Analytical, College Station, TX, USA). The filter papers were kept refrigerated in opaque bottles at around -25 °C in a refrigerator until the samples were analyzed using a portable fluorometer (model 10-AU-005-CE; Turner Designs, Sunnyvale, CA, USA), with specific wavelengths were 430 nm (blue) and 662 nm (red). In the laboratory, the filter papers were extracted with methanol to obtain Chl. *a* concentration. These samples were analyzed for less than 72 h to prevent light and chemical degradation.

2.3 Data analysis and numerical modeling

Three water quality variables (DIC, DOC, and Chl *a*) were compared between different layers (upper and lower layers), years (typhoon and non-typhoon years), and seasons (spring, summer, autumn, and winter). First, we separated our investigation data into typhoon years and non-typhoon years as described in Sect. 2.3.1. Next, we developed a conceptual equations model to generate continuous DIC and DOC data at the upper and lower layers as shown in Sect. 2.3.2 -. This helped us understand the transportation, photosynthesis, and remineralization rates between seasons and between typhoon and non-typhoon years.

2.3.1 Typhoon and non-typhoon years

We collected meteorological data from a meteorological tower located about 1.0 km from YYL (Lin et al., 2021; Lin et al., 2022). Data on rainfall (model N-68; Nippon Electric Instrument, Tokyo, Japan) and wind speed (model 03001, R.M. Young, Traverse City, MI, USA) were stored in a datalogger (model CR1000; Campbell Scientific, Logan, UT, USA) every 10 min. River discharge (Q_{in}, m^3 d^{-1}) was estimated every 10 min using the rainfall data and a water depth meter (model HOBO U20; Onset Computer, Bourne, MA, USA) at the end of a river inflow (Fig. 1) using the Manning formula. Transparency was estimated using Secchi disc data measured at local times (GMT+08:00) from 10:00 to 14:00.

As Table 1 shows, four strong typhoons were recorded, contributing a total of 2,254 mm of precipitation in all 24 months of 2015 and 2016, This accounted for 35.6% of the annual precipitation. However, no typhoon rainfall was recorded at YYL in 2017 and 2018; the total precipitation in that 2-year period was around 2,537 mm. There was no significant difference in average water depth between 2017 and 2018 (Table 1). The average discharge was less than 774

178    $m^3 \, d^{-1}$ in 2017 and 2018. Thus, we considered 2015 and 2016 as typhoon years, and 2017 and

179   2018 as non-typhoon years.

180

181   ***2.3.2   Conceptual two-layer DIC and DOC model***

182   Nakayama et al. (2010) successfully developed a conceptual two-layer dissolved oxygen

183   model based on strong wind turbulence at Tokyo Bay. Lin et al. (2021) pointed out that thermal

184   stratification that inhibits vertical C flux between the upper and lower layers in shallow stratified

185   lakes makes it possible to develop conceptual two-layer C models (Lin et al., 2022; Nakayama et

186   al., 2022). The phytoplankton and remineralization effects on DIC and DOC fluxes ($d\mathrm{DIC}/dt$ and

187    $d\mathrm{DOC}/dt$, mg-C $L^{-1} \, d^{-1}$) were considered in a conceptual two-layer equation model as shown in

188   Equations 1–4. The fluxes in the upper layer (from the water surface to 2.5 m water depth) were

189   calculated as follows:

$$V_U \frac{d\mathrm{DIC}_U}{dt} = Q_U \mathrm{DIC}_R - Q_{out}\mathrm{DIC}_U - V_U \alpha_{PU} Chl_U + V_U \alpha_{MU} DOC_U + A_I w_I (\mathrm{DIC}_L - \mathrm{DIC}_U) \tag{1}$$

$$+ Q_L \mathrm{DIC}_L - \frac{A_s F_{CO2}}{C_U} + Pa_U$$

$$V_U \frac{d\mathrm{DOC}_U}{dt} = Q_U \mathrm{DOC}_R - Q_{out}\mathrm{DOC}_U - V_U \alpha_{MU} DOC_U + A_I w_I (\mathrm{DOC}_L - \mathrm{DOC}_U) \tag{2}$$

$$+ Q_L \mathrm{DOC}_L + Pb_U$$

190   Those in the lower layer (from 2.5 to 4.0 m water depth) were calculated as follows:

$$V_L \frac{d\mathrm{DIC}_L}{dt} = Q_L \mathrm{DIC}_R - V_L \alpha_{PL} Chl_L + V_L \alpha_{ML} DOC_L + A_I w_I (\mathrm{DIC}_U - \mathrm{DIC}_L) - Q_L \mathrm{DIC}_L \tag{3}$$

$$+ \frac{A_B BF_{DIC}}{C_U} + Pa_L$$

$$V_L \frac{d\mathrm{DOC}_L}{dt} = Q_L \mathrm{DOC}_R - V_L \alpha_{ML} DOC_L + A_I w_I (\mathrm{DOC}_U - \mathrm{DOC}_L) - Q_L \mathrm{DOC}_L + Pb_L \tag{4}$$

$$V_{total} = V_U + V_L \tag{5}$$

$$Q_{in} = Q_U + Q_L \tag{6}$$

191   where, as shown in Table 2, total lake volume (V_{total}, 53,544 m^3) comprises to the upper layer

192   (V_U, 45,456 m^3) and to the lower layer (V_L, 8,808 m^3) (Equation 5), and where the lake surface

193   area (A_s) is 36,000 m^2 and the bottom of the lake area (A_B) is 3,520 m^2. The interface is 2.5 m

194   vertically, and the interface area (A_I) is 7,264 m^2 in YYL. The water depth varied from 4.56 to

195   4.66 m during the typhoon period (Chiu et al., 2020; Lin et al., 2022). Therefore, we can assume

196   that the changes in lake volumes and areas were negligible. The coefficient C_U, with a value of
197   1000, used to establish a standard unit for F_{CO2} (mg-C m^{-2} d^{-1}), considering the air–water CO_2
198   exchange by Fick's law as follows:

$$F_{CO2} = k_{CO2} \cdot K_H(pCO2_{water} - pCO2_{air}) \qquad (7)$$

199   where k_{CO2} is the gas transfer velocity from empirical wind speed equations (Cole and Caraco,
200   1998; Jähne et al., 1987; Smith, 1985; Wanninkhof, 1992). K_H is Henry's coefficient calculated
201   by water temperature empirical equations (Plummer and Busenberg, 1982). $pCO2_{air}$ (µatm) is
202   the CO_2 partial pressure in the atmosphere using air pressure data (Lin et al., 2021; Lin et al.,
203   2022), and the atmospheric CO_2 concentration is assumed to be 400 ppm. $pCO2_{water}$(µatm) is
204   the CO_2 partial pressure at the water surface around 0.04 m water depth from water quality data
205   (temperature, pH, DIC concentration at the water surface. The empirical equation (Cai and
206   Wang, 1998) was also followed by Lin et al. (2021). F_{CO2} contributed approximately half of
207   the net ecosystem production (NEP) across the water surface to the atmosphere in YYL (Lin et
208   al., 2021). Further, because sediment carbon may be an important flux into shallow subtropical
209   lakes, the sediment C flux (BF_{DIC}, BF_{DOC}, mg-C L^{-1}) in the lower layer was considered (Lin et
210   al., 2022).

211   We assumed that the river discharge and outflow discharge (Q_{out}, m^3 d^{-1}) are in a
212   quasi–steady state ($Q_{in} = Q_{out}$), divided into upper discharge (Q_U, m^3 d^{-1}) and lower discharge
213   (Q_L, m^3 d^{-1}) (Equation 6). Lin et al. (2021) showed that the buoyancy frequencies in YYL were
214   0.011 ± 0.004 s^{-1}, 0.013 ± 0.004 s^{-1}, 0.006 ± 0.003 s^{-1}, and 0.007 ± 0.004 s^{-1} from spring
215   (March–May), summer (June–August), autumn (September–November), and winter
216   (December–February), respectively, inhibiting the vertical profile of DIC mixed due to
217   stratification. We estimated the percentages of Q_U and Q_L based on the buoyancy frequency
218   following Lin et al. (2020 and 2022). Q_U values were 75%, 80%, 45%, and 50% of Q_{in} for
219   spring to winter, and Q_L values were 25%, 20%, 55%, and 50% of Q_{in}. The physical and
220   biogeochemical regimes under climate change remain uncertain, such as biological
221   compositions, mixing regimes, morphometric characteristics, and air–water energy fluxes
222   (evaporation and transpiration) (Woolway et al., 2020). To simulate extreme climate scenarios,
223   we shifted the ratio of Q_{in} for each season and tested the river intrusion hypothesis. We
224   established two extreme conditions: *Level 1* and *Level 2*. *Level 2* is the more extreme condition:
225   Q_U is 80% (spring), 85% (summer), 50% (autumn), and 50% (winter) of Q_{in}; Q_L is 20%
226   (spring), 15% (summer), 50% (autumn), and 50% (winter) of Q_{in}. *Level 1* is the condition
227   between the present and the *Level 2* condition: Q_U is 77% (spring), 82% (summer), 47%
228   (autumn), and 50% (winter) of Q_{in}; Q_L is 23% (spring), 18% (summer), 53% (autumn), and
229   50% (winter) of Q_{in} (Table 2).

230   The contributions of photosynthesis production depended on the chlorophyll *a*

231   concentration (Chl_U, Chl_L, mg L^{-1}) and on the absorption coefficients in the upper layer (α_{PU}, d^{-1})

232   ^{1}) and lower layer (α_{PL}, d^{-1}). The coefficients of DOC remineralization rates in the upper layer

233   (α_{MU}, d^{-1}) and lower layer (α_{ML}, d^{-1}) were also considered in the conceptual models. The Pa_U,

234   Pa_L, Pb_U, and Pb_L are constants in the conceptual models. To obtain unknown values (α_{PU},

235   α_{MU}, α_{PL}, α_{MU}, α_{ML}, w_I, BF_{DIC}, BF_{DOC}, Pa_U, Pa_L, Pb_U, and Pb_L), we applied multiple

236   linear regression analysis. Further, these unknown values were tested by trial and error to obtain

237   the parameters of the *best-fit* condition (Nakayama et al., 2022). The same parameters of the *best-*

238   *fit* condition were used to obtain the extreme conditions for *Level 1* and *Level 2*. We used the

239   coefficient of determination (R^2) and the Nash–Sutcliffe model efficiency coefficient (NSE)

240   (Nash and Sutcliffe, 1970) to quantify the performance of the equation model with DIC and DOC

241   sampling data (observation data) for each simulation as follows.

$$NSE = 1 - \frac{\sum_{i=1}^{n}(Obs_i - Sim_i)^2}{\sum_{i=1}^{n}(Obs_i - \overline{Obs})^2} \tag{8}$$

242   where Obs is observation data of DIC and DOC concentrations, and Sim is best-fit data for

243   conceptual model.

244

2.3.3   *DIC and DOC fluxes*

246   Net ecosystem production was defined as the difference between primary production

247   and ecological respiration (NEP = GPP - ER) due to photosynthesis and respiration via biota

248   (Dodds and Whiles, 2020). Given that we assumed that the C fluxes were dependent on the river

249   inflows in YYL (Fig. 1), we estimated the NEP by end-member analysis using the C

250   concentration of the river inflow and outflow (Lin et al., 2021; Nakayama et al., 2020) by

251   following Equations 9–12. The upper layer NEP of DIC flux (mg C d^{-1}) was obtained from

252   Equation 1 as follows:

$$\begin{aligned}
\text{Upper flux}_{DIC} &= C_U \alpha_{PU} Chl_U - C_U \alpha_{MU} DOC_U - C_U \frac{A_I w_I (\text{DIC}_L - \text{DIC}_U)}{V_U} - C_U \frac{Pa_U}{V_U} \\
&= C_U \frac{Q_U \text{DIC}_R + Q_L \text{DIC}_L - Q_{out} \text{DIC}_U}{V_U} - \frac{A_S}{V_U} F_{CO2} \\
&= C_U \frac{1}{t_{rU}} \left(\frac{Q_U}{Q_{in}} \text{DIC}_R + \frac{Q_L}{Q_{in}} \text{DIC}_L - \text{DIC}_U \right) - F_C \\
t_{rU} &= \frac{V_U}{Q_{in}}
\end{aligned} \tag{9}$$

253

254   The upper layer flux of DOC flux (mg C m^{-3} d^{-1}) was estimated from Equation 2:

$$\text{Upper flux}_{\text{DOC}} = C_U \alpha_{MU} DOC_U - C_U \frac{A_I w_I(\text{DOC}_L - \text{DOC}_U)}{V_U} - C_U \frac{Pb_U}{V_U}$$

$$= C_U \frac{Q_U \text{DOC}_R + Q_L \text{DOC}_L - Q_{out} \text{DOC}_U}{V_U} \tag{10}$$

$$= C_U \frac{1}{t_{rU}} \left(\frac{Q_U}{Q_{in}} \text{DOC}_R + \frac{Q_L}{Q_{in}} \text{DOC}_L - \text{DOC}_U \right)$$

255

256 The lower layer flux of DIC flux (mg C m^{-3} d^{-1}) was estimated from Equation 3:

$$\text{Lower flux}_{\text{DIC}} = C_U \alpha_{PL} Chl_L - C_U \alpha_{ML} DOC_L - C_U \frac{A_I w_I(\text{DIC}_U - \text{DIC}_L)}{V_L} - \frac{A_B BF_{DIC}}{V_L}$$

$$- C_U \frac{Pa_L}{V_L} = C_U \frac{Q_L(\text{DIC}_R - \text{DIC}_L)}{V_L} = C_U \frac{1}{t_{rL}} \frac{Q_L}{Q_{in}} (\text{DIC}_R - \text{DIC}_L) \tag{11}$$

$$t_{rL} = \frac{V_L}{Q_{in}}$$

257

258 The lower layer flux of DOC flux (mg C m^{-3} d^{-1}) was estimated from Equation 4:

$$\text{Lower flux}_{\text{DOC}} = C_U \alpha_{ML} DOC_L - C_U \frac{A_I w_I(\text{DOC}_U - \text{DOC}_L)}{V_L} - \frac{A_B BF_{DOC}}{V_L} - C_U \frac{Pb_L}{V_L}$$

$$= C_U \frac{Q_L(\text{DOC}_R - \text{DOC}_L)}{V_L} = C_U \frac{1}{t_{rL}} \frac{Q_L}{Q_{in}} (\text{DOC}_R - \text{DOC}_L) \tag{12}$$

259

260 Thus, the total flux of DIC and that of DOC are:

$$\text{Flux}_{\text{DIC}} = \frac{V_U \text{Upper flux}_{\text{DIC}} + V_L \text{Lower flux}_{\text{DIC}}}{V_{total}} \tag{13}$$

$$\text{Flux}_{\text{DOC}} = \frac{V_U \text{Upper flux}_{\text{DOC}} + V_L \text{Lower flux}_{\text{DOC}}}{V_{total}} \tag{14}$$

261

262 where, F_C is $\frac{A_S}{V_U} F_{CO2}$ and t_{rU}, t_{rL} are residence times (*d*) in the upper and lower layers,

263 respectively. These parameters were used for the best-fit condition as shown in Table 2.

264

3.   Results

3.1   *DIC, DOC, and Chl. a concentrations in typhoon and non-typhoon years*

The comparisons between the two typhoon years (2015 and 2016) revealed no significant differences in DIC, DOC, and Chl *a* concentrations between the upper and lower layers; however, all these parameters differed significantly between the layers in the non-typhoon years 2017 and 2018 (Fig. 2). This is because of typhoon-induced mixing and lower thermal stratification between upper and lower layer(Lin et al., 2021; Lin et al., 2022). Overall, the average DIC_U was 2.06 mg-C L^{-1}, and DIC_L was 3.66 mg-C L^{-1}; the average DOC_U was 5.87 mg-C L^{-1}, and DOC_L was 8.02 mg-C L^{-1}; and Chl_U and Chl_L were 2.13 μg-C L^{-1} and 18.5 μg-C L^{-1}, respectively. In typhoon years, the average DIC_U was 2.34 mg-C L^{-1}, and DIC_L was 4.07 mg-C L^{-1}; the average DOC_U was 6.10 mg-C L^{-1}, and DOC_L was 8.38 mg-C L^{-1}; and the Chl_U and Chl_L were 2.38 μg-C L^{-1} 12.2 μg-C L^{-1}, respectively (Fig. 2); In non-typhoon years, the average DIC_U was 1.81 mg-C L^{-1}, and DIC_L was 3.28 mg-C L^{-1}; the average DOC_U was 5.66 mg-C L^{-1}, and DOC_L was 7.67 mg-C L^{-1}; and Chl_U and Chl_L were 1.89 μg-C L^{-1} and 24.4 μg-C L^{-1}, respectively (Fig. 2).

ANOVA results indicated no significant differences in DIC concentrations among seasons during the typhoon years (*p*-values $\geq$ 0.05), suggesting a lack of statistically significant variation in DIC data across seasons (Fig. 3a–b). However, the DOC concentration showed significant differences between seasons in the typhoon years (Fig. 3c–d). No significant differences between Chl_U and Chl_L were observed among the seasons (Fig. 3e–f) , whereas the standard deviations (SD) of DIC and DOC were higher in summer and autumn (Fig. 3) due to terrestrial C loading (Chiu et al., 2020). In summer, the SD values of DIC_U and DOC_U were 3.51 mg-C L^{-1} and 3.69 mg-C L^{-1}, respectively (Fig. 3a, c, e). In autumn, DIC_L and DOC_L had the highest SD (4.06 and 4.17 mg-C L^{-1}, respectively) (Fig. 3b, d). Notably, the maximums of DIC_U and DOC_U were 7.06 and 15.6 mg-C L^{-1} and those of DIC_L and DOC_L were 10.9 and 19.8 mg-C L^{-1}, respectively, in the typhoon years (Fig. 3a-d**)**.

Positive Pearson correlations of 0.45 to 0.80 were observed between the DOC and DIC in the typhoon years (Fig. 4a). In the non-typhoon years, the upper layer DIC_L was the only variable correlated negatively with DOC in the upper and lower layers **(**Fig. 4b).DIC in the lower layer was positively correlated with the Chl_L (Fig. 4) due to the abundant respiration in the lower layer (Lin et al., 2021; Tsai et al., 2008).

3.2   *Performance of conceptual two-layer DIC and DOC models*

The results for the typhoon years demonstrated that that DIC_U was around 1.5 to 5.0 mg-C L^{-1} (Fig. 5a–b) and DIC_L was around 5.0 mg-C L^{-1} (Fig. 5d). In the non-typhoon years (2017–2018), the best-fit values of DIC_U and DIC_L were 0.40 and 0.70, respectively. On the other hand, the DOC fit our observation data (R^2 values are 0.91, and 0.46;the NSE coefficients from in equation (8) are 0.95 and 0.73) (Fig. 5e-h, Table 3). The parameters for the conceptual two-layer DIC and DOC models showed different regimes between the typhoon and non-typhoon years (Table 3). In the typhoon years, the photosynthesis absorption rate coefficients (α_{PU}, α_{PL}) were negative (photosynthesis < respiration) for each season. YYL was a C source due to a large allochthonous C loading during typhoons; the respiration was elevated by around 30- to 150-fold from summer to autumn. However, the values of the transportation coefficients (w_I) were higher in autumn than in the other seasons (Table 3). Further, the higher remineralization rates during typhoon disturbances from summer to autumn resulted in positive α_{MU} and α_{ML}. In the non-typhoon years, the remineralization rates were negative (Table 3). Thus, the results suggest that the conceptual two-layer C models may reasonably fit the observation data.

313 ### *3.3 Interannual and seasonal NEP in YYL*

314   The typhoon disturbances in summer and autumn played an important role in

315 promoting the C released by YYL (Table 4). Overall, YYL released 245 mg C m^{-3} d^{-1} of DIC

316 and 415 mg C m^{-3} d^{-1} of DOC during the typhoon years; during the non-typhoon years, it

317 released 51.7 mg C m^{-3} d^{-1} of DIC and 22.8 mg C m^{-3} d^{-1} of DOC (Table 4). The average F_C

318 was one to two times larger than $Flux_{DIC}$, and 219 and 133 mg C m^{-3} d^{-1} were released from

319 YYL into the atmosphere in the typhoon and non-typhoon years, respectively (Table 4). In

320 summer, the upper layer exhibited declines in both DIC and DOC concentrations, with the

321 decline in DIC being declined approximately 3.7 times higher more DIC in the typhoon years

322 than in the non-typhoon years (Table 4). "In autumn in the typhoon years, 216 mg C d-1 of upper

323 layer DIC was released, but 46.1 mg C m-3 d-1of upper layer DOC was produced. The upper layer

324 $Flux_{DIC}$ was negative in autumn in the typhoon years, when 268 mg C m^{-3} d^{-1} more F_C was

325 released compared to autumn in the non-typhoon years. In addition, the lower layer exhibited

326 the largest release of C into the outflow in the typhoon years; however, the flux in the lower

327 layer was more than twice as high in the summer as in the autumn of those years (Table 4). The

328 average total $Flux_{DIC}$ exhibited a release of approximately 3.14 times more C in the typhoon years

329 than in the non-typhoon years. The average total NEP_{DOC} showed an increased of 62.3 mg C m^{-3}

330 d^{-1} of DOC between the typhoon years and non-typhoon years due to the over 10-fold higher

331 flux in the upper layer (Table 4).

332

333 **_3.4_** **_Interannual responses of DIC and DOC to typhoons_**

334   We simulated the responses of DIC and DOC flux to typhoons using conceptual two-
335 layer C models. The results showed that the DIC was more sensitive to typhoon disturbances
336 than DOC under the scenarios of _Level 1_ and _Level 2_ (Fig. 6–8). Overall, the C level declined in
337 the upper layers but increased in the lower layers (Fig. 6). DIC and DOC in the upper layer
338 tended to decline from 1.0 (_Level 1_) to 2.0 mg-C L^{-1} (_Level 2_) (Fig. 7a, c); however, they
339 increased to 10.0 and 20.0 mg-C L^{-1} in the lower layer under _Level 1_ and _Level 2_, respectively
340 (Fig. 6b, d).

341   The DIC concentration in the upper layer was significantly lower in the typhoon years
342 than in the non-typhoon years during spring and autumn under _Level 2_ (Fig. 7a–c). Under the
343 _best-fit_ and _Level 1_ conditions, the DIC concentrations decreased significantly from winter to
344 spring (Fig. 7c-d). The lower layer DIC values under the _best-fit_ and _Level 1_ conditions differed
345 significantly between the typhoon and non-typhoon years (Fig. 7e–h). The DIC of the lower
346 layer under _Level 2_ differed significantly from winter to spring only (Fig. 7e, h). The highest
347 averaged DIC in the lower layer   was 10 mg-C L^{-1} under the _Level 2_ in spring in non-typhoon
348 years (Fig 7e).

349   The upper layer DOC showed significant typhoon responses for each condition from
350 winter to spring (Fig. 8a, d). The DOC of the upper layer tended to differ more significantly
351 under the extreme climates from summer to autumn (Fig. 8b–c). The DOC of the lower layer
352 showed different typhoon responses between spring and the other seasons (Fig. 8e–h), and the
353 DOC values in the lower layer under _Level 2_ conditions in spring showed no significant
354 difference between the typhoon and non-typhoon years (Fig 8e).

355

4.   Discussion

4.1   Biochemical and physical differences of DIC and DOC fluxes between typhoon and non-typhoon-years in YYL

Annual total precipitation was 40% higher in the typhoon years than in the non-typhoon years (Table 1).Water retention and typhoon-induced upwelling control the dynamics of DIC and DOC during the summer and autumn (Chiu et al., 2020; Jones et al., 2009; Tsai et al., 2008; Tsai et al., 2011). The absence of typhoon-induced upwelling affected water quality data differences between the upper and lower layers (Chiu et al., 2020; Lin et al., 2022; Tsai et al., 2008; Tsai et al., 2011). DIC, DOC, and Chl. *a* concentrations differed significantly between upper and lower layers in the non-typhoon years (Fig. 2). Further, the abundance of microorganisms leads to intensive respirations in the lower layers during the non-typhoon period in YYL; for example, an anoxic condition at the hypolimnion may decrease the efficiency of C mineralization and remineralization rates in non-typhoon years (Carey et al., 2022; Chiu et al., 2020; Lin et al., 2022; Shade et al., 2010; Shade et al., 2011). Therefore, these physical and biogeochemical processes might describe different patterns between the upper and lower layers (Fig. 4).

Thermal stratification and allochthonous C loading may drive the responses of fluxes to typhoons in YYL.The absolute values of fluxes were higher in the typhoon years than in the non-typhoon years (Table 4). We found that precipitation from typhoons loaded large amounts of allochthonous C into YYL during summer and autumn, which might explain the higher fluxes in autumn compared to the other seasons (Table 4). Typhoons dramatically changed the seasonal and interannual patterns of DIC fluxes due to river intrusion (Fig. 6a–b; Fig. 7), which proves to our hypothesis and corresponds to the results of previous studies (Chiu et al., 2020; Lin et al., 2021; Lin et al., 2022). In summer, the spatial differences between layers in DIC and DOC were inhibited due to strong thermal stratification, describing the positive upper net primary production and lower negative net primary production (Lin et al., 2021).The thermal stratification and anoxic condition may have been controlled by the seasonal and interannual patterns of DIC and DOC fluxes in the non-typhoon years (Tables 3–4; Fig. 5).

Because of the absence of typhoon-induced mixing and allochthonous C loading, the total fluxes were lower in the non-typhoon years than those in the typhoon years (Table 4). In the typhoon years, our results showed that typhoon-induced upwelling and loading increased by 102.2 mg-DIC m^{-3} d^{-1} and 62.3 mg-DOC m^{-3} d^{-1} in YYL (Table 4). Additionally, the CO_2 emission (F_C) was 43 % higher (~83 mg C m^{-3} d^{-1}) in the typhoon years than in the non-typhoon years (Table 4). Therefore, typhoon disturbances control DIC loading and C emissions in YYL, consistent with our previous studies (Chiu et al., 2020; Lin et al., 2021; Lin et al., 2022). Simultaneously, bio-photochemical mineralization and degradation may play a key role in

392 shaping C fluxes because colored DOC reduces ultraviolet radiation (UVR) and active

393 photosynthetic radiation (PAR) (Allesson et al., 2021; Chiu et al., 2020; Schindler et al., 1996;

394 Scully et al., 1996; Williamson et al., 1999), resulting in the higher light intensity and water

395 temperature in summer consuming 3.7 times more DIC and DOC than in the other seasons

396 (Table 4) These results suggested that the allochthonous C loading and light duration might be

397 the most crucial factor for DIC and DOC fluxes in the typhoon years. Conversely, the

398 transportation rate shaped the seasonal C concentrations due to thermal stratification in the non-

399 typhoon years.

400

401 *4.2   Model limitation under the extreme weather scenarios*

402   Water temperature might be a crucial driver in controlling C fluxes in YYL (Chiu et

403 al., 2020; Lin et al., 2021; Lin et al., 2022). We found that the fluxes and F_{CO2} in summer were

404 usually higher than in winter (Tables 3–4) due to the higher levels of photosynthesis,

405 remineralization, and thermal stratification strength (Lin et al., 2021; Lin et al., 2022). With the

406 conceptual two-layer C models (Table 3), photosynthesis absorption (α_{PU}, α_{PL}),

407 remineralization (α_{MU}, α_{ML}), and transportation (w_I) well represented the seasonal variations in

408 DIC and DOC data. These parameters of the conceptual two-layer C models appeared in

409 reasonable patterns (Table 3). The higher remineralization and photosynthesis rates resulted in

410 higher absolute values of fluxes in the autumn of the typhoon years (Tables 3–4). In the non-

411 typhoon years, the photosynthesis rates contributed to the total fluxes (Tables 3–4). Moreover,

412 without the typhoon-induced mixing and refreshing of the water column, anoxic conditions may

413 occur (Carey et al., 2022; Vachon et al., 2021), which could result in negative remineralization

414 rates in non-typhoon years. Thus, the conceptual two-layer C models well characterizes the

415 seasonal and interannual responses of DIC and DOC fluxes to typhoons in YYL.

416   Under extreme weather conditions, *Level 2* usually shifted to different typhoon

417 responses for each season (Fig. 7–8) due to extreme river intrusions. DIC changes more

418 significantly than DOC under *Level 1* and *Level 2* (Fig. 6-8), because the photosynthesis,

419 transportation, and remineralization rates may crucially affect the seasonal and interannual

420 patterns of DOC as well. Moreover, we compared the fluxes with different model conditions as

421 shown in Fig. 9, demonstrating that the responses of Flux$_{DIC}$ to typhoons differed dramatically

422 between *Level 1* and *Level 2* (Fig. 9a-c); especially, the Upper Flux$_{DIC}$ released more C in the

423 typhoon years and absorbed more C in the non-typhoon years than *Obs* (Fig. 9a). Not only were

424 the absolute values of Flux$_{DIC}$ over 3 times higher in the typhoon years than in the non-typhoon

425 years (Table 4), but SD was higher in the typhoon years as well (Fig. 9). However, DOC fluxes

426 changed less under *Level 1* and *Level 2* (Fig. 9d–f), a finding that is consistent with our

427 continuous DOC data (Fig. 7c–d). Processes such as respiration, mineralization, and sediment

428 burial may impact DOC fluxes (Bartosiewicz et al., 2015; Hanson et al., 2015; Maranger et al.,

429 2018).Ejarque et al. (2021) also successfully developed a conceptual one-layer model of DOC

430 and DIC, considering bacterial respiration, photo-mineralization and degradation in a temperate

431 mountain lake. In addition, Nagatomo et al. (2023) suggested that DIC might be underestimated

432 if submerged vegetation is ignored. Thus, we suggest that photo-biochemical processes (such as

433 photo-mineralization) and submerged vegetation should be considered in the upper layer to

434 clarify and validate the responses of the total C fluxes under extreme climates in a two-layer

435 stratified lake.

5.   Conclusions

We successfully developed two-layer conceptual C models to obtain continuous DIC and DOC data in YYL and to simulate extreme conditions. Our conceptual two-layer C model revealed that allochthonous and autochthonous processes both accounted for C flux responses to typhoon disturbances . Without typhoons, thermal stratification was the primary driver of seasonal and interannual patterns of DIC and DOC. In the typhoon years, the changes in seasonal river intrusion regimes in YYL resulted in a 3-fold higher total $Flux_{DIC}$ than in the non-typhoon years. However, our model should be improved for application to extreme climate scenarios by considering other autochthonous processes, such as sediment burial, photo-biochemical processes, and anoxic conditions. The present results suggest that physical processes (river intrusion and vertical transportation) and biogeochemical processes (mineralization, photosynthesis, and respiration) in a subtropical small lake account for the C flux responses to typhoons on seasonal and interannual time scales.

Competing interests

The authors have no conflicts of interest to report.

Acknowledgements

The authors thank YS Hsueh, LC Jiang, and TY Chen for their help with the water sample collection and chemistry analysis. This work was supported by the Japan Society for the Promotion of Science (JSPS) under grant nos. 22H05726, 22H01601, and 18KK0119 to K Nakayama; and by the Academia Sinica, Taiwan (AS-103-TP-B15), Ministry of Science and Technology, Taiwan (MOST 106-2621-M-239-001, MOST 107-2621-M-239-001, MOST 108-2621-M-239-001) to CY Chiu and JW Tsai. This study benefited from participation in the Global Lakes Ecological Observatory Network (GLEON).

Hao-Chi Lin: Conceptualization, Methodology, Investigation, Formal analysis, Writing – original draft. Keisuke Nakayama: Methodology, Supervision, Writing – review & editing, Conceptualization. Jeng-Wei Tsai: Investigation, Funding acquisition, Writing –review & editing. Chih-Yu Chiu: Funding acquisition, Writing – review & editing.

Data availability

The data that support the findings of this study are adopted from our previous works, including Chiu et al. (2020), Lin et al. (2021), and Lin et al. (2022).

471 **References**

472 Allesson, L., Koehler, B., Thrane, J.-E., Andersen, T., and Hessen, D. O.: The role of
473   photomineralization for CO_2 emissions in boreal lakes along a gradient of dissolved organic
474   matter, Limnol. Oceanogr., 66, 158–170, https://doi.org/10.1002/lno.11594, 2021.

475 Amaral, J. H. F., Melack, J. M., Barbosa, P. M., Borges, A. V., Kasper, D., Cortés, A. C., Zhou,
476   W., MacIntyre, S., and Forsberg, B. R.: Inundation, Hydrodynamics and Vegetation
477   Influence Carbon Dioxide Concentrations in Amazon Floodplain Lakes, Ecosystems, 25,
478   911–930, https://doi.org/10.1007/s10021-021-00692-y, 2022.

479 Aufdenkampe, A. K., Mayorga, E., Raymond, P. A., Melack, J. M., Doney, S. C., Alin, S. R.,
480   Aalto, R. E., and Yoo, K.: Riverine coupling of biogeochemical cycles between land,
481   oceans, and atmosphere, Front. Ecol. Environ., 9, 53–60, https://doi.org/10.1890/100014,
482   2011.

483 Bartosiewicz, M., Laurion, I., and MacIntyre, S.: Greenhouse gas emission and storage in a
484   small shallow lake, Hydrobiologia, 757, 101–115, https://doi.org/10.1007/s10750-015-2240-
485   2, 2015.

486 Cai, W.-J. and Wang, Y.: The chemistry, fluxes, and sources of carbon dioxide in the estuarine
487   waters of the Satilla and Altamaha Rivers, Georgia, Limnol. Oceanogr., 43, 657–668,
488   https://doi.org/10.4319/lo.1998.43.4.0657, 1998.

489 Carey, C. C., Hanson, P. C., Thomas, R. Q., Gerling, A. B., Hounshell, A. G., Lewis, A. S. L.,
490   Lofton, M. E., McClure, R. P., Wander, H. L., Woelmer, W. M., Niederlehner, B. R., and
491   Schreiber, M. E.: Anoxia decreases the magnitude of the carbon, nitrogen, and phosphorus
492   sink in freshwaters, Glob. Change Biol., https://doi.org/10.1111/gcb.16228, 2022.

493 Chang, S.-C., Wang, C.-P., Feng, C.-M., Rees, R., Hell, U., and Matzner, E.: Soil fluxes of
494   mineral elements and dissolved organic matter following manipulation of leaf litter input in
495   a Taiwan Chamaecyparis forest, For. Ecol. Manag., 242, 133–141,
496   https://doi.org/10.1016/j.foreco.2007.01.025, 2007.

497 Chiu, C.-Y., Jones, J. R., Rusak, J. A., Lin, H.-C., Nakayama, K., Kratz, T. K., Liu, W.-C., Tang,
498   S.-L., and Tsai, J.-W.: Terrestrial loads of dissolved organic matter drive inter-annual carbon
499   flux in subtropical lakes during times of drought, Sci. Total Environ, 717, 137052,
500   https://doi.org/10.1016/j.scitotenv.2020.137052, 2020.

501 Chou, C.-H., Chen, T.-Y., Liao, C.-C., and Peng, C.-I.: Long-term ecological research in the
502   Yuanyang Lake forest ecosystem I. Vegetation composition and analysis, Bot. Bull. Acad.
503   Sin., 41, 61–72, 2000.

504 Cole, J. J. and Caraco, N. F.: Atmospheric exchange of carbon dioxide in a low-wind

505 oligotrophic lake measured by the addition of SF_6, Limnol. Oceanogr., 43, 647–656,

506 https://doi.org/10.4319/lo.1998.43.4.0647, 1998.

507 Cole, J. J., Prairie, Y. T., Caraco, N. F., McDowell, W. H., Tranvik, L. J., Striegl, R. G., Duarte,

508 C. M., Kortelainen, P., Downing, J. A., Middelburg, J. J., and Melack, J.: Plumbing the

509 Global Carbon Cycle: Integrating Inland Waters into the Terrestrial Carbon Budget,

510 Ecosystems, 10, 172–185, https://doi.org/10.1007/s10021-006-9013-8, 2007.

511 Czikowsky, M. J., MacIntyre, S., Tedford, E. W., Vidal, J., and Miller, S. D.: Effects of Wind

512 and Buoyancy on Carbon Dioxide Distribution and Air-Water Flux of a Stratified Temperate

513 Lake, J. Geophys. Res. Biogeosci., 123, 2305–2322, https://doi.org/10.1029/2017JG004209,

514 2018.

515 Dodds, W. K. and Whiles, M. R.: Freshwater Ecology: Concepts and Environmental

516 Applications of Limnology, Third Edition, Elsevier, United Kingdom, 748-762, 2020.

517 Doubek, J. P., Anneville, O., Dur, G., Lewandowska, A. M., Patil, V. P., Rusak, J. A., Salmaso,

518 N., Seltmann, C. T., Straile, D., Urrutia-Cordero, P., Venail, P., Adrian, R., Alfonso, M. B.,

519 DeGasperi, C. L., Eyto, E., Feuchtmayr, H., Gaiser, E. E., Girdner, S. F., Graham, J. L.,

520 Grossart, H.-P., Hejzlar, J., Jacquet, S., Kirillin, G., Llames, M. E., Matsuzaki, S.-I. S.,

521 Nodine, E. R., Piccolo, M. C., Pierson, D. C., Rimmer, A., Rudstam, L. G., Sadro, S., Swain,

522 H. M., Thackeray, S. J., Thiery, W., Verburg, P., Zohary, T., and Stockwell, J. D.: The extent

523 and variability of storm-induced temperature changes in lakes measured with long-term and

524 high-frequency data, Limnol. Oceanogr., 66, 1979–1992, https://doi.org/10.1002/lno.11739,

525 2021.

526 Douville, H., Raghavan, K., Renwick, J., Allan, R. P., Arias, P. A., Barlow, M., Cerezo-Mota, R.,

527 Cherchi, A., Gan, T. Y., Gergis, J., Jiang, D., Khan, A., Mba, W. P., Rosenfeld, D., Tierney,

528 J., and Zolina, O.: Water cycle changes, Cambridge University Press, Climate Change 2021:

529 The Physical Science Basis. Contribution of Working Group I to 45 the Sixth Assessment

530 Report of the Intergovernmental Panel on Climate Change, 2021.

531 Downing, J. A., Prairie, Y. T., Cole, J. J., Duarte, C. M., Tranvik, L. J., Striegl, R. G.,

532 McDowell, W. H., Kortelainen, P., Caraco, N. F., Melack, J. M., and Middelburg, J. J.: The

533 global abundance and size distribution of lakes, ponds, and impoundments, Limnol.

534 Oceanogr., 51, 2388–2397, https://doi.org/10.4319/lo.2006.51.5.2388, 2006.

535 Ejarque, E., Scholz, K., Wohlfahrt, G., Battin, T. J., Kainz, M. J., and Schelker, J.: Hydrology

536 controls the carbon mass balance of a mountain lake in the eastern European Alps, Limnol.

537 Oceanogr., 66, 2110–2125, https://doi.org/10.1002/lno.11712, 2021.

538 Engel, F., Farrell, K. J., McCullough, I. M., Scordo, F., Denfeld, B. A., Dugan, H. A., Eyto, E.

539 de, Hanson, P. C., McClure, R. P., Nõges, P., Nõges, T., Ryder, E., Weathers, K. C., and

540 Weyhenmeyer, G. A.: A lake classification concept for a more accurate global estimate of

the dissolved inorganic carbon export from terrestrial ecosystems to inland waters, Sci. Nat., 105, 25, https://doi.org/10.1007/s00114-018-1547-z, 2018.

Hanson, P. C., Pace, M. L., Carpenter, S. R., Cole, J. J., and Stanley, E. H.: Integrating Landscape Carbon Cycling: Research Needs for Resolving Organic Carbon Budgets of Lakes, Ecosystems, 18, 363–375, https://doi.org/10.1007/s10021-014-9826-9, 2015.

Hope, D., Palmer, S. M., Billett, M. F., and Dawson, J. J. C.: Variations in dissolved CO_2 and CH_4 in a first-order stream and catchment: an investigation of soil-stream linkages, Hydrol. Process., 18, 3255–3275, https://doi.org/10.1002/hyp.5657, 2004.

Jähne, B., Münnich, K. O., Bösinger, R., Dutzi, A., Huber, W., and Libner, P.: On the parameters influencing air-water gas exchange, J. Geophys. Res. Oceans, 92, 1937, https://doi.org/10.1029/JC092iC02p01937, 1987.

Jones, S. E., Kratz, T. K., Chiu, C.-Y., and McMahon, K. D.: Influence of typhoons on annual CO_2 flux from a subtropical, humic lake, Glob. Change Biol., 15, 243–254, https://doi.org/10.1111/j.1365-2486.2008.01723.x, 2009.

Kimura, N., Liu, W.-C., Chiu, C.-Y., and Kratz, T.: The influences of typhoon-induced mixing in a shallow lake, Lakes Reserv.: Res. Manag., 17, 171–183, https://doi.org/10.1111/j.1440-1770.2012.00509.x, 2012.

Kimura, N., Liu, W.-C., Tsai, J.-W., Chiu, C.-Y., Kratz, T. K., and Tai, A.: Contribution of extreme meteorological forcing to vertical mixing in a small, shallow subtropical lake, J. Limnol., 76, 116–128, https://doi.org/10.4081/jlimnol.2016.1477, 2017.

Kossin, J. P., Olander, T. L., and Knapp, K. R.: Trend Analysis with a New Global Record of Tropical Cyclone Intensity, J. Clim., 26, 9960–9976, https://doi.org/10.1175/JCLI-D-13-00262.1, 2013.

Kraemer, B. M., Pilla, R. M., Woolway, R. I., Anneville, O., Ban, S., Colom-Montero, W., Devlin, S. P., Dokulil, M. T., Gaiser, E. E., Hambright, K. D., Hessen, D. O., Higgins, S. N., Jöhnk, K. D., Keller, W., Knoll, L. B., Leavitt, P. R., Lepori, F., Luger, M. S., Maberly, S. C., Müller-Navarra, D. C., Paterson, A. M., Pierson, D. C., Richardson, D. C., Rogora, M., Rusak, J. A., Sadro, S., Salmaso, N., Schmid, M., Silow, E. A., Sommaruga, R., Stelzer, J. A. A., Straile, D., Thiery, W., Timofeyev, M. A., Verburg, P., Weyhenmeyer, G. A., and Adrian, R.: Climate change drives widespread shifts in lake thermal habitat, Nat. Clim. Chang., 11, 521–529, https://doi.org/10.1038/s41558-021-01060-3, 2021.

Lai, I.-L., Chang, S.-C., Lin, P.-H., Chou, C.-H., and Wu, J.-T.: Climatic Characteristics of the Subtropical Mountainous Cloud Forest at the Yuanyang Lake Long-Term Ecological Research Site, Taiwan, Taiwania, 51, 317–329, 2006.

Lauerwald, R., Laruelle, G. G., Hartmann, J., Ciais, P., and Regnier, P. A.: Spatial patterns in CO_2 evasion from the global river network, Global Biogeochem. Cycles, 29, 534–554,

577   https://doi.org/10.1002/2014GB004941, 2015.

578 Lin, H.-C., Chiu, C.-Y., Tsai, J.-W., Liu, W.-C., Tada, K., and Nakayama, K.: Influence of

579   Thermal Stratification on Seasonal Net Ecosystem Production and Dissolved Inorganic

580   Carbon in a Shallow Subtropical Lake, J. Geophys. Res. Biogeosci., 126,

581   https://doi.org/10.1029/2020JG005907, 2021.

582 Lin, H.-C., Tsai, J.-W., Tada, K., Matsumoto, H., Chiu, C.-Y., and Nakayama, K.: The impacts

583   of the hydraulic retention effect and typhoon disturbance on the carbon flux in shallow

584   subtropical mountain lakes, Sci. Total Environ, 803, 150044,

585   https://doi.org/10.1016/j.scitotenv.2021.150044, 2022.

586 Maberly, S. C., O'Donnell, R. A., Woolway, R. I., Cutler, M. E. J., Gong, M., Jones, I. D.,

587   Merchant, C. J., Miller, C. A., Politi, E., Scott, E. M., Thackeray, S. J., and Tyler, A. N.:

588   Global lake thermal regions shift under climate change, Nat Commun., 11, 1232,

589   https://doi.org/10.1038/s41467-020-15108-z, 2020.

590 MacIntyre, S., Bastviken, D., Arneborg, L., Crowe, A. T., Karlsson, J., Andersson, A., Gålfalk,

591   M., Rutgersson, A., Podgrajsek, E., and Melack, J. M.: Turbulence in a small boreal lake:

592   Consequences for air-water gas exchange, Limnol. Oceanogr., 66, 827–854,

593   https://doi.org/10.1002/lno.11645, 2021.

594 Maranger, R., Jones, S. E., and Cotner, J. B.: Stoichiometry of carbon, nitrogen, and phosphorus

595   through the freshwater pipe, Limnol Oceanogr Lett, 3, 89–101,

596   https://doi.org/10.1002/lol2.10080, 2018.

597 Marcé, R., Obrador, B., Gómez-Gener, L., Catalán, N., Koschorreck, M., Arce, M. I., Singer, G.,

598   and Schiller, D. von: Emissions from dry inland waters are a blind spot in the global carbon

599   cycle, Earth-Sci. Rev., 188, 240–248, https://doi.org/10.1016/j.earscirev.2018.11.012, 2019.

600 Nagatomo, K., Nakayama, K., Komai, K., Matsumoto, H., Watanabe, K., Kubo, A., Tada, K.,

601   Maruya, Y., Yano, S., Tsai, J. W., Lin, H. C., Vilas, M., and Hipsey, M. R.: A Spatially

602   Integrated Dissolved Inorganic Carbon (SiDIC) Model for Aquatic Ecosystems Considering

603   Submerged Vegetation, J Geophys Res Biogeosci, 128,

604   https://doi.org/10.1029/2022JG007032, 2023.

605 Nakayama, K., Kawahara, Y., Kurimoto, Y., Tada, K., Lin, H.-C., Hung, M.-C., Hsueh, M.-L.,

606   and Tsai, J.-W.: Effects of oyster aquaculture on carbon capture and removal in a tropical

607   mangrove lagoon in southwestern Taiwan, Sci. Total Environ, 156460,

608   https://doi.org/10.1016/j.scitotenv.2022.156460, 2022.

609 Nakayama, K., Komai, K., Tada, K., Lin, H. C., Yajima, H., Yano, S., Hipsey, M. R., and Tsai, J.

610   W.: Modeling dissolved inorganic carbon considering submerged aquatic vegetation, Ecol.

611   Model., 431, 109188, https://doi.org/10.1016/j.ecolmodel.2020.109188, 2020.

612 Nakayama, K., Sivapalan, M., Sato, C., and Furukawa, K.: Stochastic characterization of the

613   onset of and recovery from hypoxia in Tokyo Bay, Japan: Derived distribution analysis

614   based on "strong wind" events, Water Resour. Res., 46,

615   https://doi.org/10.1029/2009WR008900, 2010.

616 Nash, J. E. and Sutcliffe, J. V.: River flow forecasting through conceptual models, I A discussion

617   of principles, J. Hydrol., 10, 398–409, 1970.

618 Olsson, F., Mackay, E. B., Barker, P., Davies, S., Hall, R., Spears, B., Exley, G., Thackeray, S.

619   J., and Jones, I. D.: Can reductions in water residence time be used to disrupt seasonal

620   stratification and control internal loading in a eutrophic monomictic lake?, J. Environ.

621   Manage., 304, 114169, https://doi.org/10.1016/j.jenvman.2021.114169, 2022a.

622 Olsson, F., Mackay, E. B., Moore, T., Barker, P., Davies, S., Hall, R., Spears, B., Wilkinson, J.,

623   and Jones, I. D.: Annual water residence time effects on thermal structure: A potential lake

624   restoration measure?, J. Environ. Manage., 314, 115082,

625   https://doi.org/10.1016/j.jenvman.2022.115082, 2022b.

626 Plummer, L. and Busenberg, E.: The solubilities of calcite, aragonite and vaterite in CO_2-H_2O

627   solutions between 0 and 90°C, and an evaluation of the aqueous model for the system

628      $CaCO_3$-CO_2-H_2O, Geochim. Cosmochim. Acta, 46, 1011–1040,

629   https://doi.org/10.1016/0016-7037(82)90056-4, 1982.

630 Raymond, P. A., Hartmann, J., Lauerwald, R., Sobek, S., McDonald, C., Hoover, M., Butman,

631   D., Striegl, R., Mayorga, E., Humborg, C., Kortelainen, P., Dürr, H., Meybeck, M., Ciais, P.,

632   and Guth, P.: Global carbon dioxide emissions from inland waters, Nature, 503, 355–359,

633   https://doi.org/10.1038/nature12760, 2013.

634 Schindler, D. W., Curtis, P. J., Parker, B. R., and Stainton, M. P.: Consequences of climate

635   warming and lake acidification for UV-B penetration in North American boreal lakes,

636   Nature, 379, 705–708, https://doi.org/10.1038/379705a0, 1996.

637 Scully, N. M., McQueen, D. J., and Lean, D. R. S.: Hydrogen peroxide formation: The

638   interaction of ultraviolet radiation and dissolved organic carbon in lake waters along a 43-

639   75°N gradient, Limnol. Oceanogr., 41, 540–548, https://doi.org/10.4319/lo.1996.41.3.0540,

640   1996.

641 Shade, A., Chiu, C.-Y., and McMahon, K. D.: Seasonal and episodic lake mixing stimulate

642   differential planktonic bacterial dynamics, Microb. Ecol., 59, 546–554,

643   https://doi.org/10.1007/s00248-009-9589-6, 2010.

644 Shade, A., Read, J. S., Welkie, D. G., Kratz, T. K., Wu, C. H., and McMahon, K. D.: Resistance,

645   resilience and recovery: aquatic bacterial dynamics after water column disturbance, Environ.

646   Microbiol., 13, 2752–2767, https://doi.org/10.1111/j.1462-2920.2011.02546.x, 2011.

647 Shih, Y.-T., Chen, P.-H., Lee, L.-C., Liao, C.-S., Jien, S.-H., Shiah, F.-K., Lee, T.-Y., Hein, T.,

648   Zehetner, F., Chang, C.-T., and Huang, J.-C.: Dynamic responses of DOC and DIC transport

649   to different flow regimes in a subtropical small mountainous river, Hydrol. Earth Syst. Sci.,

650   22, 6579–6590, https://doi.org/10.5194/hess-22-6579-2018, 2019.

651 Smith, S. V.: Physical, chemical and biological characteristics* of CO_2 gas flux across the air-

652   water interface, Plant Cell Environ., 8, 387–398, https://doi.org/10.1111/j.1365-

653   3040.1985.tb01674.x, 1985.

654 Sobek, S., Tranvik, L. J., and Cole, J. J.: Temperature independence of carbon dioxide

655   supersaturation in global lakes, Global Biogeochem. Cycles, 19, GB2003,

656   https://doi.org/10.1029/2004GB002264, 2005.

657 Sun, P., He, S., Yu, S., Pu, J., Yuan, Y., and Zhang, C.: Dynamics in riverine inorganic and

658   organic carbon based on carbonate weathering coupled with aquatic photosynthesis in a

659   karst catchment, Southwest China, Water Research, 189, 116658,

660   https://doi.org/10.1016/j.watres.2020.116658, 2021.

661 Tranvik, L. J., Downing, J. A., Cotner, J. B., Loiselle, S. A., Striegl, R. G., Ballatore, T. J.,

662   Dillon, P., Finlay, K., Fortino, K., Knoll, L. B., Kortelainen, P. L., Kutser, T., Larsen, S.,

663   Laurion, I., Leech, D. M., McCallister, S. L., McKnight, D. M., Melack, J. M., Overholt, E.,

664   Porter, J. A., Prairie, Y., Renwick, W. H., Roland, F., Sherman, B. S., Schindler, D. W.,

665   Sobek, S., Tremblay, A., Vanni, M. J., Verschoor, A. M., Wachenfeldt, E. von, and

666   Weyhenmeyer, G. A.: Lakes and reservoirs as regulators of carbon cycling and climate,

667   Limnol. Oceanogr., 54, 2298–2314, https://doi.org/10.4319/lo.2009.54.6_part_2.2298, 2009.

668 Tsai, J.-W., Kratz, T. K., Hanson, P. C., Kimura, N., Liu, W.-C., Lin, F.-P., Chou, H.-M., Wu, J.-

669   T., and Chiu, C.-Y.: Metabolic changes and the resistance and resilience of a subtropical

670   heterotrophic lake to typhoon disturbance, Can. J. Fish. Aquat. Sci., 68, 768–780,

671   https://doi.org/10.1139/F2011-024, 2011.

672 Tsai, J.-W., Kratz, T. K., Hanson, P. C., Wu, J.-T., Chang, W. Y. B., Arzberger, P. W., Lin, B.-S.,

673   Lin, F.-P., Chou, H.-M., and Chiu, C.-Y.: Seasonal dynamics, typhoons and the regulation of

674   lake metabolism in a subtropical humic lake, Freshw. Biol., 53, 1929–1941,

675   https://doi.org/10.1111/j.1365-2427.2008.02017.x, 2008.

676 Vachon, D. and Del Giorgio, P. A.: Whole-Lake CO_2 Dynamics in Response to Storm Events in

677   Two Morphologically Different Lakes, Ecosystems, 17, 1338–1353,

678   https://doi.org/10.1007/s10021-014-9799-8, 2014.

679 Vachon, D., Sponseller, R. A., and Karlsson, J.: Integrating carbon emission, accumulation and

680   transport in inland waters to understand their role in the global carbon cycle, Glob. Change

681   Biol., 27, 719–727, https://doi.org/10.1111/gcb.15448, 2021.

682 Wanninkhof, R.: Relationship between wind speed and gas exchange over the ocean, J.

683   Geophys. Res. Oceans, 97, 7373, https://doi.org/10.1029/92JC00188, 1992.

684 Williamson, C. E., Morris, D. P., Pace, M. L., and Olson, O. G.: Dissolved organic carbon and

685   nutrients as regulators of lake ecosystems: Resurrection of a more integrated paradigm,

686   Limnol. Oceanogr., 44, 795–803, https://doi.org/10.4319/lo.1999.44.3_part_2.0795, 1999.

687 Winslow, L. A., Read, J. S., Hansen, G. J. A., and Hanson, P. C.: Small lakes show muted

688   climate change signal in deepwater temperatures, Geophys. Res. Lett., 42, 355–361,

689   https://doi.org/10.1002/2014GL062325, 2015.

690 Woolway, R. I., Anderson, E. J., and Albergel, C.: Rapidly expanding lake heatwaves under

691   climate change, Environ. Res. Lett., 16, 94013, https://doi.org/10.1088/1748-9326/ac1a3a,

692   2021a.

693 Woolway, R. I., Jennings, E., Shatwell, T., Golub, M., Pierson, D. C., and Maberly, S. C.: Lake

694   heatwaves under climate change, Nature, 589, 402–407, https://doi.org/10.1038/s41586-

695   020-03119-1, 2021b.

696 Woolway, R. I., Kraemer, B. M., Lenters, J. D., Merchant, C. J., O'Reilly, C. M., and Sharma,

697   S.: Global lake responses to climate change, Nat. Rev. Earth Environ., 1, 388–403,

698   https://doi.org/10.1038/s43017-020-0067-5, 2020.

699 Woolway, R. I., Simpson, J. H., Spiby, D., Feuchtmayr, H., Powell, B., and Maberly, S. C.:

700   Physical and chemical impacts of a major storm on a temperate lake: a taste of things to

701   come?, Climatic Change, 151, 333–347, https://doi.org/10.1007/s10584-018-2302-3, 2018.

702 Wu, J.-T., Chang, S.-C., Wang, Y.-S., and Hsu, M.-K.: Characteristics of the acidic environment

703   of the Yuanyang Lake (Taiwan), Bot. Bull. Acad. Sin., 42, 17–22, 2001.

704 Zhou, Y., Yu, X., Zhou, L., Zhang, Y., Xu, H., Zhu, M., Zhu, G., Jang, K.-S., Spencer, R. G. M.,

705   Jeppesen, E., Brookes, J. D., Kothawala, D. N., and Wu, F.: Rainstorms drive export of

706   aromatic and concurrent bio-labile organic matter to a large eutrophic lake and its major

707   tributaries, Water Research, 229, 119448, https://doi.org/10.1016/j.watres.2022.119448,

708   2023.

709 Zwart, J. A., Sebestyen, S. D., Solomon, C. T., and Jones, S. E.: The Influence of Hydrologic

710   Residence Time on Lake Carbon Cycling Dynamics Following Extreme Precipitation

711   Events, Ecosystems, 20, 1000–1014, https://doi.org/10.1007/s10021-016-0088-6, 2017.

712

713 **Table 1.** Comparison of Yuan-Yang Lake's rainfall and hydrological records in typhoon and non-
714 typhoon years.

Records	Typhoon years	Non-typhoon years
Time period (year)	2015-2016	2017-2018
Total precipitation (mm)	6,332	3,795
Total typhoon rainfall (mm)	2,254	0
Average water depth (m ± SD)	4.54 ± 1.7	4.51 ± 1.5
Average river discharge ($m^3 d^{-1}$)	3,717	2,943
Transparency (Secchi disc depth, m ± SD)	1.58 ± 0.45	1.38 ± 0.28

715

716 **Table 2.** Parameters of the two-layer conceptual model in Yuan-Yang Lake

	Parameters	Value	Unit
Measurements			
Q_{out}	Outflow discharge	Daily data	m^3 d^{-1}
Q_{in}	Inflow discharge	Daily data	m^3 d^{-1}
Q_U	Upper layer discharge	Daily data	m^3 d^{-1}
Q_L	Lower layer discharge	Daily data	m^3 d^{-1}
DIC_R	River inflow DIC	Monthly data	mg-C L^{-1}
DIC_U	Upper layer DIC	Monthly data	mg-C L^{-1}
DIC_L	Lower layer DIC	Monthly data	mg-C L^{-1}
Chl_U	Upper layer Chl *a*	Monthly data	mg L^{-1}
Chl_L	Lower layer Chl *a*	Monthly data	mg L^{-1}
DOC_U	Upper layer DOC	Monthly data	mg-C L^{-1}
DOC_L	Lower layer DOC	Monthly data	mg-C L^{-1}
F_{CO2}	Carbon emission (equation 7)	Monthly data	mg-C m^2 d^{-1}
Constants			
V_{total}	Total lake volume	53,544	m^3
V_U	Upper layer volume	45,456	m^3
V_L	Lower layer volume	8,808	m^3
A_s	Lake surface area	36,000	m^2
A_I	Interface area	7,264	m^2
A_B	Bottom of lake area	3,520	m^2
C_U	Coefficient of the standard unit	1,000	L m^{-3}
Unknow Constants			
α_{PU}, α_{PL}	Coefficients of photosynthesis	Constant	d^{-1}
α_{MU}, α_{ML}	Coefficients of mineralization	Constant	d^{-1}
w_I	Coefficient of vertical transportation	Constant	d^{-1}
BF_{DIC}, BF_{DOC}	Sediment DIC and DOC emission	Constant	mg-C L^{-1}
Pa_U, Pb_L	Equations constant at lower layer	Constant	mg m^{-3} d^{-1}
Extreme scenarios		Q_U	Q_L
Level 1	Best-fit scenario but change upper- and lower-layers discharges (Q_U, Q_L)	77% (spring), 82% (summer), 47% (autumn), 50% (winter) of Q_{in}	23% (spring), 18% (summer), 53% (autumn), 50% (winter) of Q_{in}.

			80% (spring),	20% (spring),
Level 2	Best-fit scenario but change upper and lower layers discharges (Q_U, Q_L)		85% (summer), 50% (autumn), 50% (winter) of Q_{in}	15% (summer), 50% (autumn), 50% (winter) of Q_{in}.

717

718 **Table 3.** Best-fit parameters of a two-layer conceptual model of DIC and DOC in Yuan-Yang
719 Lake from 2015 to 2018.

	2015–2016 Typhoon years				2017–2018 Non-typhoon years			
	Spring	*Summer*	*Autumn*	*Winter*	*Spring*	*Summer*	*Autumn*	*Winter*
Upper layer								
F_{CO2} (mg-C m^2 d^{-1})	291	245	422	127	231	143	104	175
α_{PU} (d^{-1})	-1.20	-33.1	-183.5	-29.1	8.0	6.0	30.0	7.77
α_{MU} (d^{-1})	-0.0227	0.0203	0.08	-0.031	-0.01	-0.039	-0.033	-0.195
w_I (d^{-1})	0.230	0.172	1.38	0.30	0.10	0.0478	0.120	0.180
Pa_U (d^{-1})	12560	-1317	-23750	9597	9880	14000	17600	10100
Pb_U (d^{-1})	-21930	9461	-42130	-17070	-3630	-1251	-20820	-9289
$d\text{DIC}_U$ (R^2, NSE)			0.305, 0.614					
$d\text{DOC}_U$ (R^2, NSE)			0.909, 0.953					
Lower layer								
α_{PL} (d^{-1})	-0.627	-22.1	15.0	-0.878	1.49	-6.87	6.0	-16.6
α_{ML} (d^{-1})	-0.025	0.123	0.0755	0.00973	-0.010	-0.0376	-0.04	-0.048
Pa_L (d^{-1})	100	-5662	-10500	-1013	151.6	2032	1216	909
Pb_L (d^{-1})	-6012	-7395	-53940	-9639	-1338	-6296	-19470	-8748
BF_{DIC}, BF_{DOC} (mg-C L^{-1})			0.04, 0.00					
$d\text{DIC}_L$ (R^2, NSE)			0.452, 0.707					
$d\text{DOC}_L$ (R^2, NSE)			0.460, 0.728					

720

721 **Table 4.** Seasonal averages of carbon fluxes (mg C m^{-3} d^{-1}) for each season in Yuan-Yang Lake.

722 Positive values are shown in the carbon sink, and negative ones show the values after carbon was

723 released.

		Flux (mg C m^{-3} d^{-1})			Total (mg C m^{-3} d^{-1})	
		F_C	Upper	Lower	Flux$_{DIC}$	Flux$_{DOC}$
Typhoon years	**Average**	**-219**	-	-	**-150**	**-9.69**
Spring	DIC	-231	-243	-45.2	-210	62.1
	DOC	-	70.8	17.2		
Summer	DIC	-194	29.1	-313	-26.4	18.8
	DOC	-	118	-495		
Autumn	DIC	-351	-216	-659	-288	-151
	DOC	-	46.1	-1167		
Winter	DIC	-100	-96.4	36.5	-74.8	31.2
	DOC	-	40.5	-16.9		
Non-typhoon years	**Average**	**-133**	-	-	**-47.8**	**52.6**
Spring	DIC	-129	-180	-94.9	-166	-7.06
	DOC	-	21.4	-67.1		
Summer	DIC	-183	5.80	-58.1	-4.57	73.8
	DOC	-	115	-140		
Autumn	DIC	-82.6	95.0	35.9	85.5	95.9
	DOC	-	168	-272		
Winter	DIC	-138	-128	6.04	-106	33.7
	DOC	-	34.0	32.1		

724

725

726
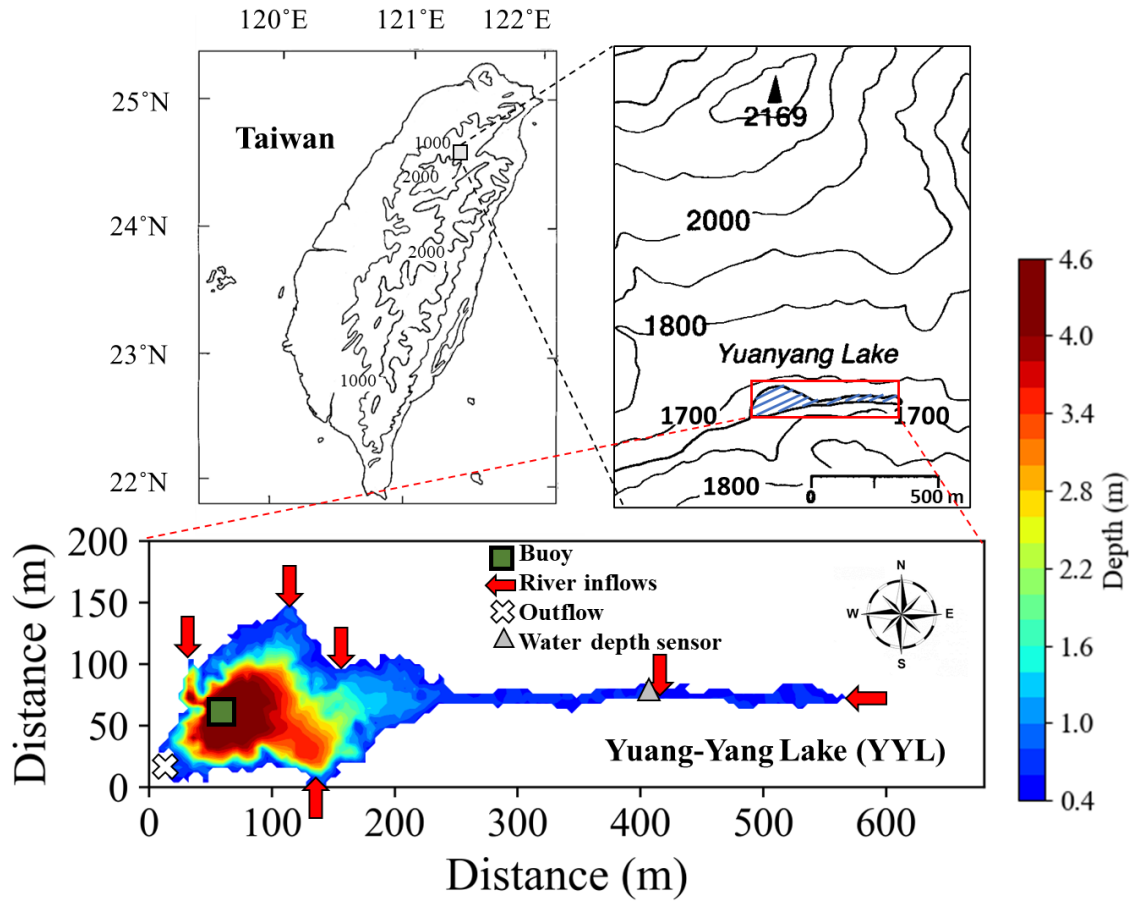
727 **Fig. 1**. Sampling locations and bathymetry maps of Yuan–Yang Lake (YYL). The dark
728 green rectangle shows the buoy station, which is located at the deepest site of the lake.
729 The *red points* and *white cross* show the river mouths of the inflows and outflows,
730 respectively. The *gray triangle* shows the location of the water depth sensor.
731

732
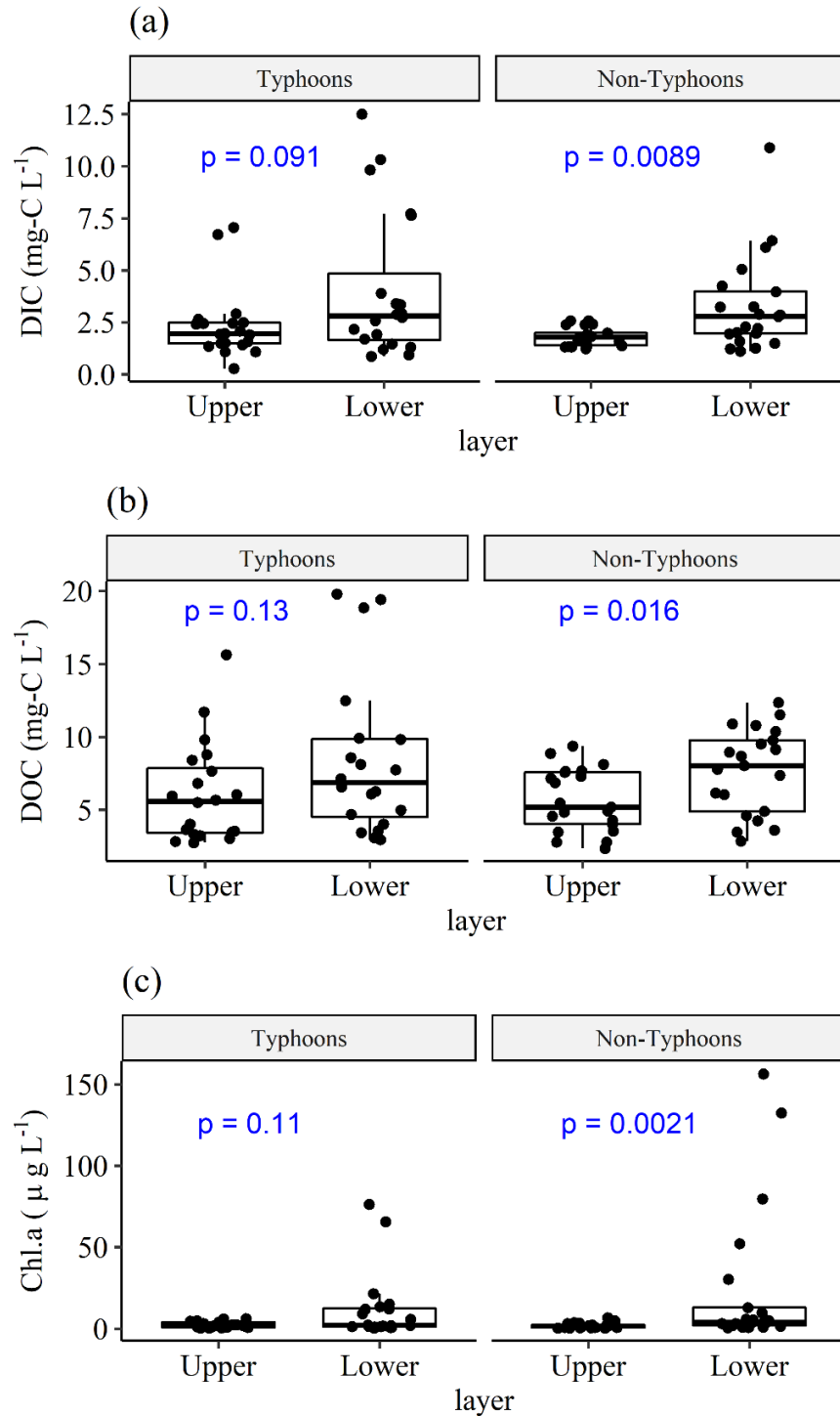
733 **Fig. 2**. Comparisons of **(a)** DIC, **(b)** DOC, and **(c)** Chl *a* between upper (DIC_U, DOC_U,

734 Chl_U) and lower (DIC_L, DOC_L, Chl_L) layers, grouped by typhoon and non-typhoon

735 years. *Bullet points* show the water sampling data. We used a t-test to obtain the *p*-

736 values (*blue texts*).
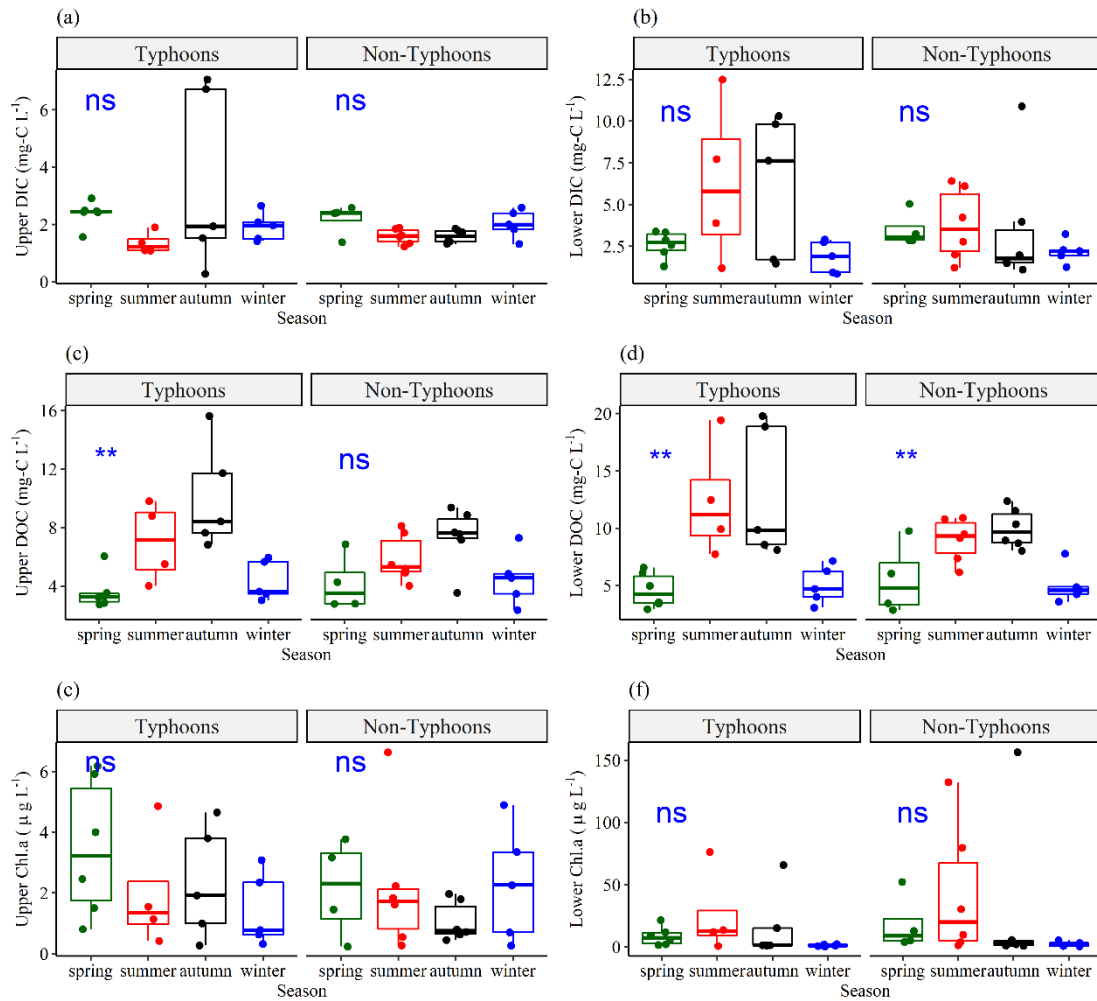
737
738 **Fig. 3.** Seasonal variations of **(a)** upper layer DIC (DIC_U), **(b)** lower layer DIC (DIC_L),
739 **(c)** upper layer DOC (DOC_U), **(d)** lower layer DOC (DOC_L), **(e)** upper layer Chl. a
740 (Chl_U), **(f)** lower layer Chl. *a* (Chl_L) grouped by typhoon and non-typhoon years. The
741 bullet points show the water sampling data. To determine seasonality, we used one-way
742 ANOVA to obtain the *p*-values. "ns**":** *p*-values $\geq$ 0.05; ***** show *p*-values from 0.05 to
743 0.01: ****:** *p*-values from 0.01 to 0.001.
744

745
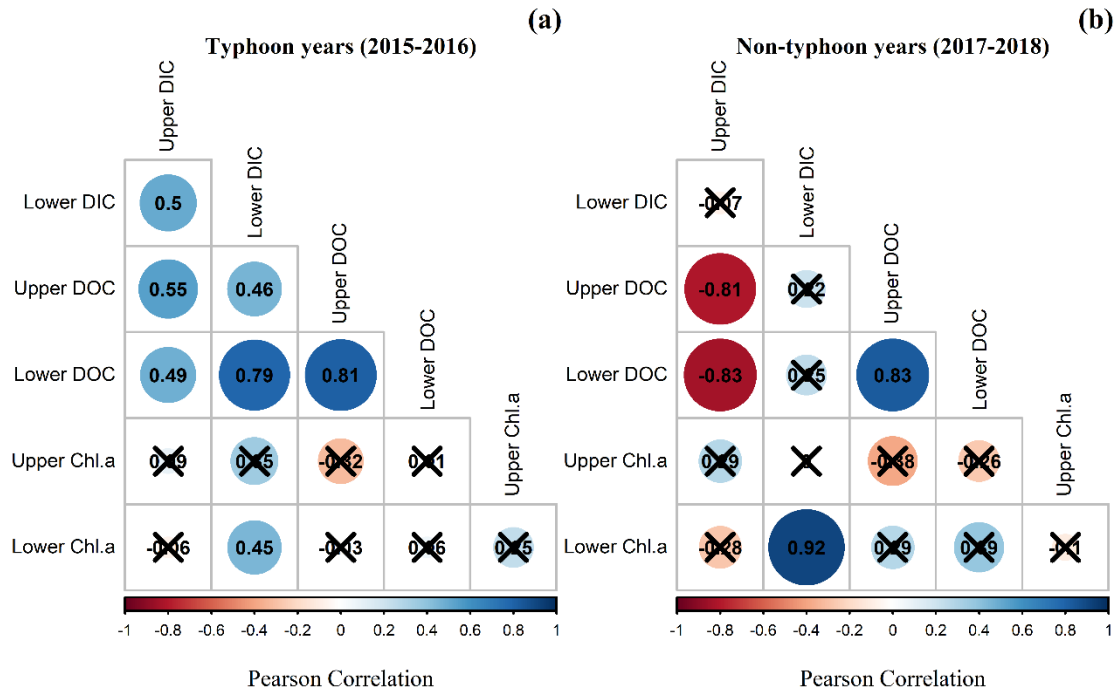
746   **Fig. 4.** Pearson correlation coefficients of DIC, DOC, and Chl. *a* concentration at upper

747   layer and lower layer DIC (DIC_U, DIC_L), DOC (DOC_U, DOC_L), Chl. a (Chl_U, Chl_L)

748   during **(a)** typhoon years and **(b)** non-typhoon years. *Black-crosses* show insignificant

749   values (*p*-values are > 0.05).

750

751

752
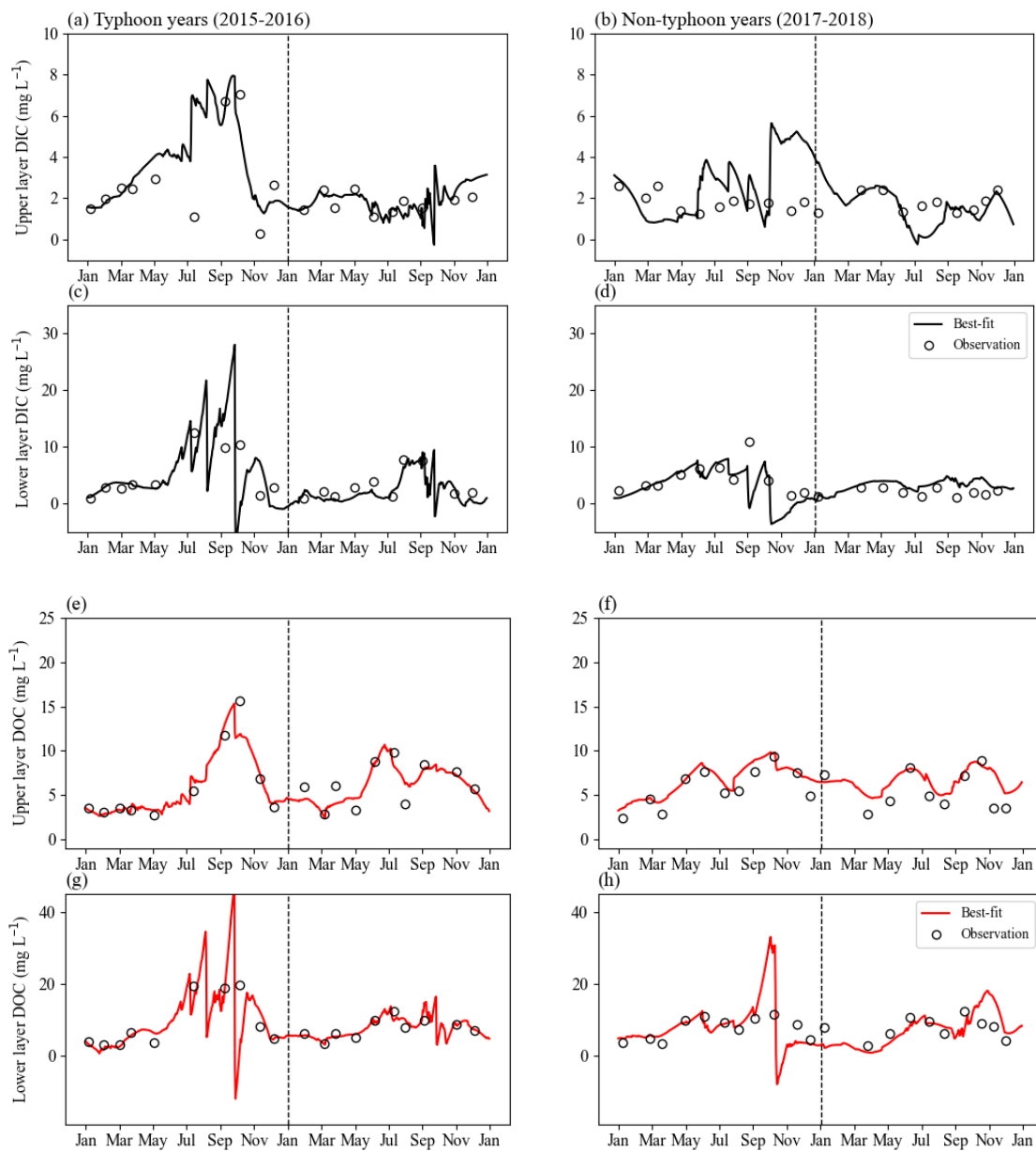
Fig. 5. Continuous daily DIC and DOC data at **(a, b, e, f)** upper layer (DIC_U, DOC_U) and **(c, d, g, h)** lower layer (DIC_L, DOC_L) by using conceptual equations models. The *black lines* show the *best fit* for DIC, *red lines* show the *best-fit* for DOC (**Table 3**), and *empty dots* show water sampling (observation) data for each month.

757

758
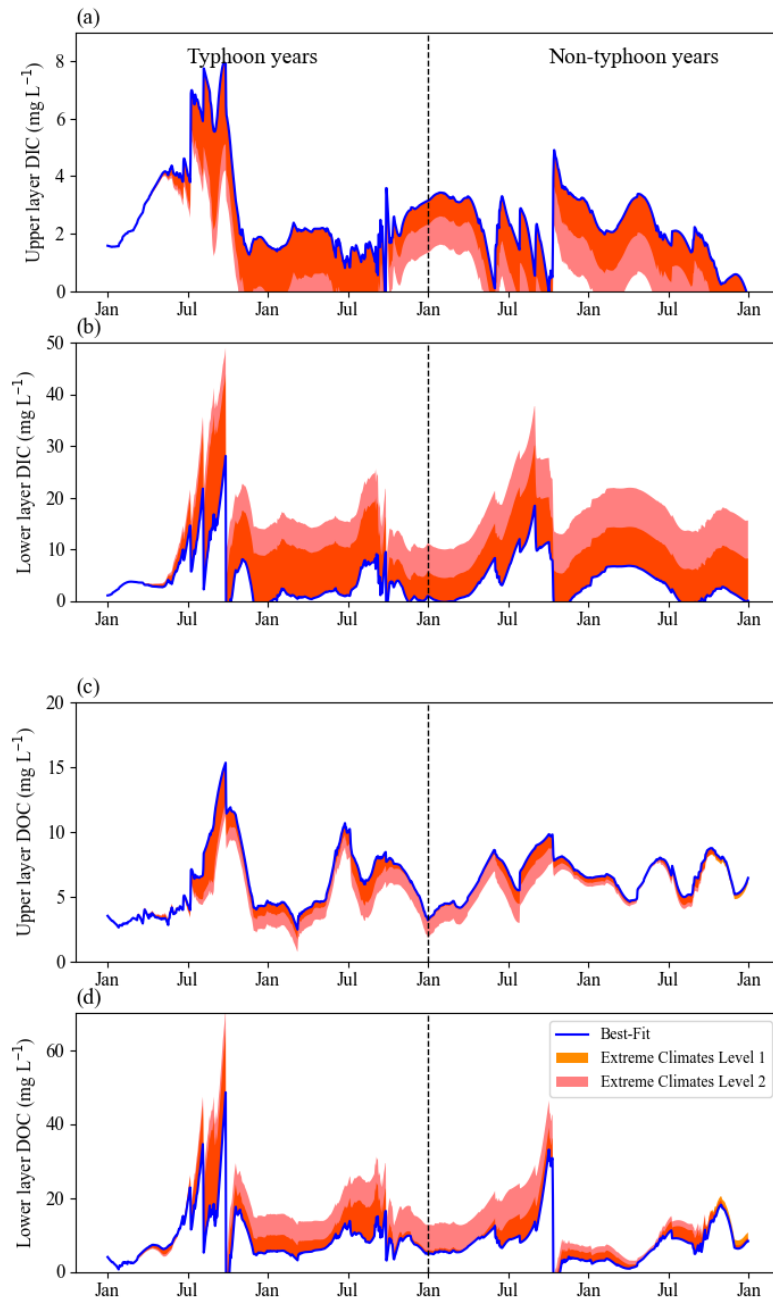
Fig. 6. Continuous daily DIC and DOC data at (**a, c**) upper layer (DIC_U, DOC_U) and (**b, d**) lower layer (DIC_L, DOC_L) by using the conceptual equation model under extreme climates from 2015 to 2018. *Blue lines* are original best-fit data as in Fig. 6, in which the parameters of the DIC model in non-typhoon years are as shown in Table 3. *Orange regions* show *Level 1*; *pink regions* show *Level 2*.
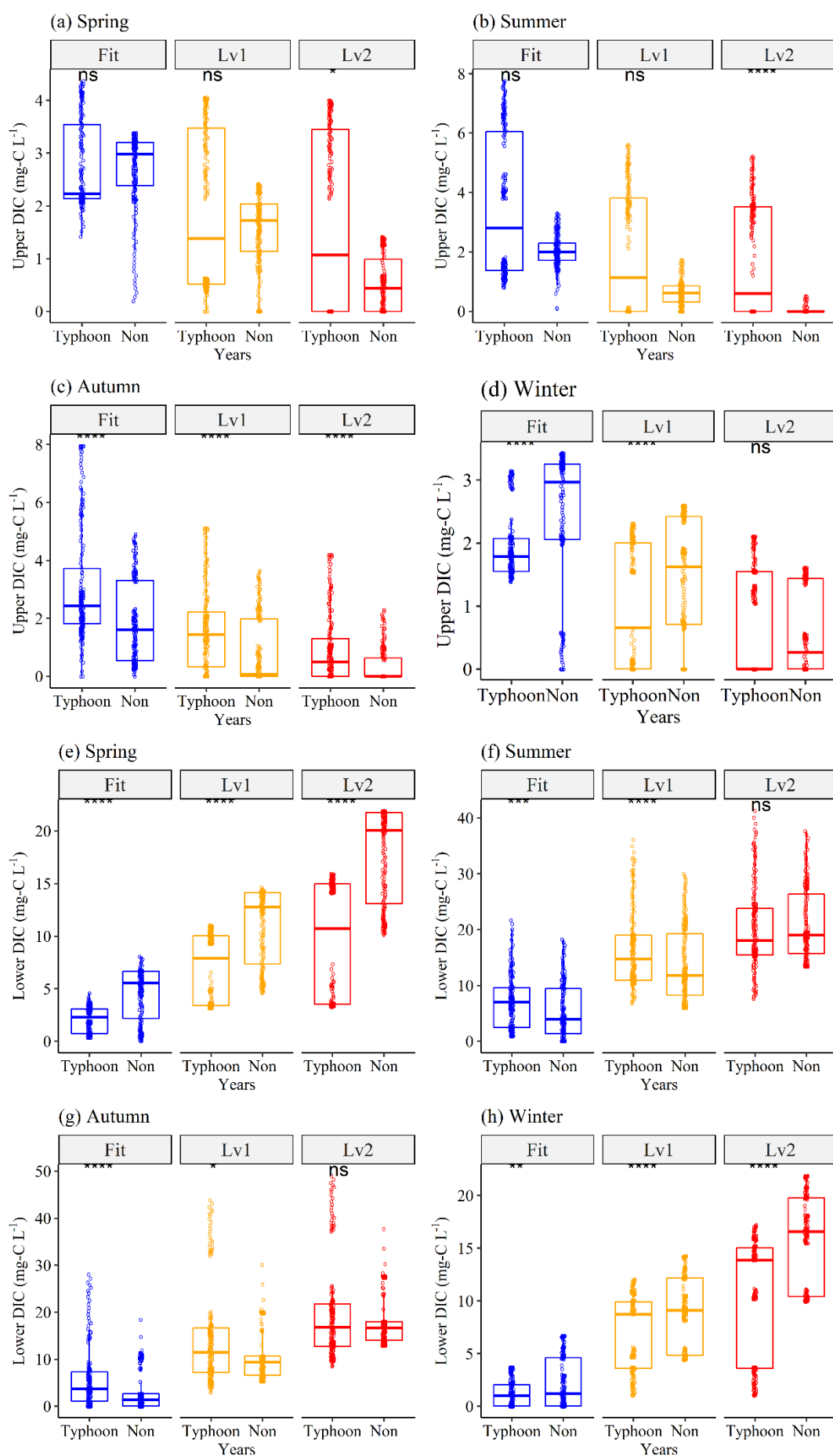
765   **Fig. 7.** Seasonal responses of continuous **(a-d)** upper layer DIC and **(e-h)** lower layer DIC

766   (mg-C L^{-1}) between typhoon (*Typhoon*) and non-typhoon (*Non*) years for each season as

767   in **Fig. 3**. *Fit* (*blue boxes*) condition shows the best-fit data by using the conceptual two-

768   layer C model; *Lv1* (*yellow boxes*) and *Lv2* (*red boxes*) show the extreme climates. Empty

769   dots show the continuous DIC and DOC data. "ns": *p*-values ≥ 0.05; *****: *p*-values from

770   0.05 to 0.01; ******: *p*-values from 0.01 to 0.001; ********: *p*-values less than 0.0001 based on a

771   t-test.
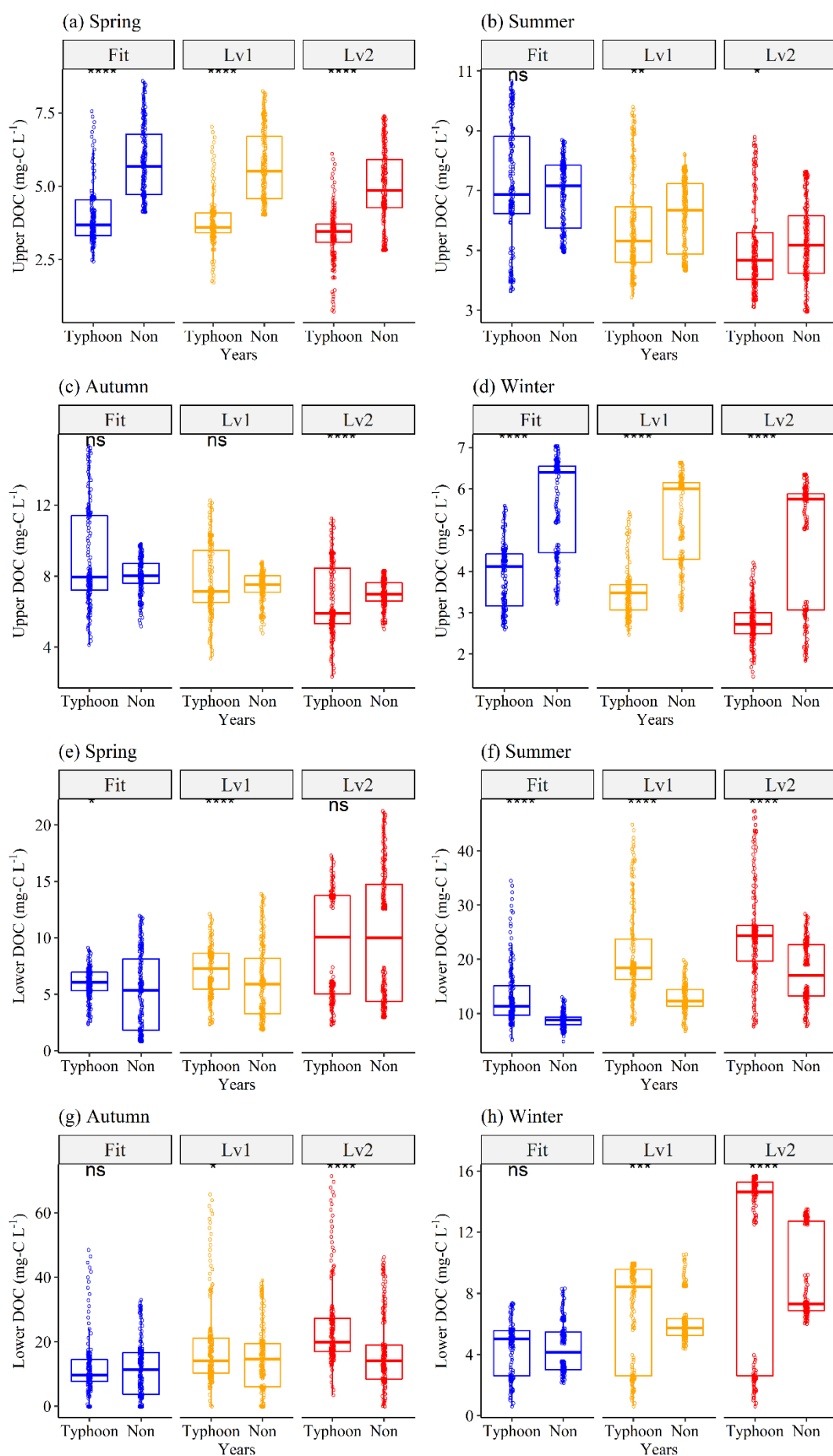
773 **Fig. 8.** Seasonal responses of **(a-d)** upper layer DOC and **(e-h)** lower layer DOC (mg-C
774 L^{-1}) between typhoon (*Typhoon*) and non-typhoon (*Non*) years for each season as in Fig.
775 7. The *Fit* (*blue boxes*) condition shows the best-fit data by using the conceptual two-
776 layer carbon model; *Lv1* (*yellow boxes*) and *Lv2* (*red boxes*) show the extreme climates.
777 Empty dots show the continuous DIC and DOC data. "ns": *p*-values ≥ 0.05; *****: *p*-values
778 from 0.05 to 0.01; ******: *p*-values from 0.01 to 0.001; ********: *p*-values less than 0.0001 based
779 on a t-test.
780

Fig. 9. Interannual (a) Upper flux$_{DIC}$, (b) Lower flux$_{DIC}$, (c) Flux$_{DIC}$, (d) Upper flux$_{DOC}$, (e) Lower flux$_{DOC}$, and (f) Flux$_{DOC}$ (mg C m^{-3} d^{-1}) grouped by typhoon and non-typhoon years. The *Obs* condition (*black boxes*) show the observation data as in Fig. 5. The *Fit* condition (*blue- boxes*) shows the best-fit data by using the conceptual two-layer carbon model as in Fig.5. *Level 1* (*yellow boxes*) and *Level 2* (*red boxes*) show the extreme scenarios as in Fig. 6. For the definitions of fluxes please see Sect. 2.3.3.